

Ideal, Defective, and Gold–Promoted Rutile $\text{TiO}_2(110)$ Surfaces: Structures, Energies, Dynamics, and Thermodynamics from PBE+U

Matteo Farnesi Camellone,* Piotr M. Kowalski,[†] and Dominik Marx
Lehrstuhl für Theoretische Chemie, Ruhr-Universität Bochum, 44780 Bochum, Germany
 (Dated: October 27, 2018)

Extensive first principles calculations are carried out to investigate gold-promoted $\text{TiO}_2(110)$ surfaces in terms of structure optimizations, electronic structure analyses, *ab initio* thermodynamics calculations of surface phase diagrams, and *ab initio* molecular dynamics simulations. All computations rely on density functional theory in the generalized gradient approximation (PBE) and account for on-site Coulomb interactions via inclusion of a Hubbard correction, PBE+U, where U is computed from linear response theory. This approach is validated by investigating the interaction between $\text{TiO}_2(110)$ surfaces and typical probe species (H, H_2O , CO). Relaxed structures and binding energies are compared to both data from the literature and plain PBE results, thus allowing the performance of the PBE+U approach for the specific purpose to be verified. The main focus of the study is on the properties of gold-promoted titania surfaces and their interactions with CO. Both PBE+U and PBE optimized structures of Au adatoms adsorbed on stoichiometric and reduced TiO_2 surfaces are computed, along with their electronic structure. The charge rearrangement induced by the adsorbates at the metal/oxide contact are also analyzed in detail and discussed. By performing PBE+U *ab initio* molecular dynamics simulations, it is demonstrated that the diffusion of Au adatoms on the stoichiometric surface is highly anisotropic. The metal atoms migrate either along the top of the bridging oxygen rows, or around the area between these rows, from one bridging position to the next along the [001] direction. No translational motion perpendicular to this direction is observed. Approximate *ab initio* thermodynamics predicts that under O-rich conditions, structures obtained by substituting a Ti_{5c} atom with an Au atom are thermodynamically stable over a wide range of temperatures and pressures that are relevant to applications in the realm of catalysis. Finally, it is shown that $\text{TiO}_2(110)$ surfaces containing positively charged Au ions activate molecular CO, whereas a single negatively charged $\text{Au}^{-\delta}$ species bound to an O vacancy only weakly interacts with CO. Despite this, the calculations predict that the reactivity of gold nanoparticles nucleated at O vacancies can be recovered for cluster sizes as small as Au_2 .

PACS numbers: 68.43.Fg, 73.20.Hb, 68.47.Gh, 82.65.+r

I. INTRODUCTION

Titania, TiO_2 , is a metal oxide of both fundamental interest and technological importance^{1–5}. It is used in several key technologies including pigments, coatings, electronic devices, implants, gas sensors, photochemical reactions, and catalysis^{6–8}. One of the most important properties of titania is that it can be easily reduced (see e.g. Ref. 9 for a concise presentation), strongly affecting its chemical properties in general and its reactivity in particular¹⁰. One way to reduce the TiO_2 surface is to remove surface oxygen atoms, thereby creating O vacancies. The removal of an O atom gives rise to two excess electrons and the appearance of new electronic states within the band gap at about 0.7 to 0.9 eV below the conduction band edge, thus creating an *F*-center^{2,3,11,12}. By this process, two substrate Ti^{4+} ions change formally to a Ti^{3+} oxidation state; see Ref. 13 for recent literature and a detailed picture of the (de-)localization dynamics of the excess electrons. Alternatively, the TiO_2 surface can be reduced by hydroxylation of surface O atoms via adsorption of hydrogen^{14–18}. The interaction of TiO_2 with water is an important process which has to be taken into account, since it occurs easily, even in well-controlled UHV experiments. The adsorption of water on TiO_2 has been investigated extensively, both experimentally and

theoretically^{9,10,19–36}; in particular see Refs. 10,19 for the most recent reviews of this literature.

Most relevant to catalysis is the interaction of Au and CO with stoichiometric or reduced TiO_2 surfaces and, in particular, the interaction of titania-supported gold particles with CO molecules. A detailed understanding of the process of CO adsorption is required to best comprehend its wide variety of applications^{2,3}, such as CO oxidation at low temperature¹², the water gas shift reaction, and CO hydrogenation^{37,38}. In a recent paper³⁹, we investigated the interaction of CO with the stoichiometric $\text{TiO}_2(110)$ surface using a combination of density functional theory (DFT) and post Hartree-Fock methods. For a single CO molecule in the (4×2) surface unit cell of our slab, we found that the upright position above the fivefold coordinated Ti sites, Ti_{5c} , remains the preferential adsorption geometry, even without enforcing symmetry. On the reduced titania surface, results from temperature-programmed desorption (TPD) experiments^{40,41} suggested that, at low coverages, CO adsorption occurs at non-adjacent Ti_{5c} sites. These findings were supported by various calculations^{42–44}. However, earlier studies implicated bridge-bonded oxygen vacancies as adsorption sites for CO^{45,46}, a conclusion corroborated by some theoretical investigations^{47,48} as well.

The seminal work of Haruta and coworkers⁴⁹ has

shown that the low-temperature oxidation of molecular CO can be efficiently catalyzed by highly dispersed Au nanoparticles supported on TiO₂ surfaces^{50–53}. It is now recognized that gold nanoclusters, prepared in different ways and supported on various metal oxides, are able to catalyze a number of reactions^{54,55}, and that the size of the gold particles substantially affects the catalytic activity. The gold clusters should be smaller than about 5 nm for high catalytic activity to occur, suggesting the key importance of metal/support interfacial interactions on a nanometer scale. Extensive studies of the Au/TiO₂ system link the peculiar catalytic activity of gold nanoparticles on titania to several factors: high concentration of low-coordination sites^{56,57}, quantum size effects of two-layer Au islands⁵⁸, active perimeter sites of the nanoparticles⁵⁹, and charge transfer between the gold particles and the supporting oxide^{52,60}.

Over the past decade, DFT-based calculations have been extensively employed to study the interaction between gold and the TiO₂(110) surface^{7,61–71}. Most of the existing theoretical studies provide information on stable adsorption sites of Au on the stoichiometric and reduced titania studies, while less effort has been devoted to the study of the O-rich Au/TiO₂(110) system^{70,71} and the diffusion of Au adatoms on the stoichiometric and reduced TiO₂(110) surface^{7,67,68}. A wide variation in the lowest-energy positions of Au on titania are reported in the literature⁶³, which can be explained in part by considering that Au can diffuse rather easily on the stoichiometric surface⁶⁷. The potential energy surface (PES) of a single Au adatom deposited on the stoichiometric TiO₂(110) surface or adsorbed into a surface O vacancy has been explored using static calculations⁶⁷. It has been shown that Au migration on the stoichiometric surface is two-dimensional, with a relatively flat profile. In the scenario where an Au atom is substituted for a surface Ti_{5c} site, it has been demonstrated that the Au atom is capable of weakening bonds of surface oxygens with the oxide⁷¹.

Most of the density functional theory studies available in the literature dealing with defects and/or molecules adsorbed on titania substrates using reasonably sized supercells make use of local (LDA) or semilocal (GGA) functionals. Despite widespread use, such functionals are known to often (but not always⁹) fail to predict qualitatively correct electronic structures for reduced transition metal oxides, due to the self-interaction error inherent in the functionals. To partially correct for the self-interaction error, different computational methods can be used: perturbative many-body theories such as “GW”^{72–74}, LDA plus dynamical mean field theory (DMFT)⁷⁵, pseudo self-interaction-correction schemes (pSIC)⁷⁶, LDA plus U⁷⁷, and other methods that rely on hybrid functionals⁷⁸. Recently, GGA+U approaches have been applied with promising results in studies of intrinsic electron transport in TiO₂ bulk^{79,80} and in the investigation of the charge (de-)localization dynamics induced by surface oxygen vacancies on the (110) surface

of TiO₂ in the rutile structure¹³. Within the GGA+U approach, the electronic structure is partially corrected for the self-interaction error by adding a Hubbard term acting on the Ti-3*d* orbitals. This approach has the advantage of not adding much computational overhead to a standard GGA calculation in the plane wave / pseudopotential framework, thus enabling one to use fairly large supercells in order to allow structural relaxation to occur or to carry out *ab initio* dynamics.

In this article, the PBE+U formalism is employed to investigate the structural and electronic properties of gold-supported TiO₂(110) surface catalysts and their reactivity towards CO. As a first step, the PBE+U approach is applied to study the interaction between the stoichiometric or reduced TiO₂(110) surface and small probe species: H, H₂O, and CO. The PBE+U structures and binding energies are compared to both the corresponding plain PBE results and reference data in the literature in order to assess the applicability of the PBE+U approach for the present purpose. When it comes to gold on titania, our PBE+U *ab initio* molecular dynamics simulations extend existing static relaxations and nudged elastic band mappings of the PES and demonstrate that Au adatoms diffuse in a highly directional manner on the stoichiometric surface. The metal atoms migrate easily, either along on top of the bridging oxygen rows or around the area between these rows, from one bridging position to the next, along the [001] direction. The relative thermodynamic stability of different TiO₂(110) structures is furthermore studied by employing the formalism of approximate *ab initio* thermodynamics. Our calculations greatly extend existing studies and show that under O-rich conditions, the thermodynamically most stable structure is the defective Au@V_{Ti5c} surface structure (obtained by substituting a surface Ti_{5c} atom with an Au adatom), while under Ti-rich conditions, the Au adatoms are preferentially adsorbed at O vacancies.

The remainder of the paper is organized as follows: In Section II the model system, the methods and the computational details are summarized. The PBE+U formalism is validated in Section III by studying the interaction of the TiO₂(110) surfaces with a set of well-studied adsorbates such as H, H₂O and CO. The main part of the paper is Section IV which presents novel insights into the structures, electronic properties, thermodynamics and dynamics of gold-promoted rutile TiO₂(110) surfaces and their interaction with CO. The concluding Section VI summarizes the main results and puts them in a broader perspective.

II. METHODS AND COMPUTATIONAL DETAILS

The TiO₂(110) surfaces were modeled by four O – Ti₂O₂ – O trilayer (4x2) supercell slabs separated by more than 10 Å of vacuum space normal to the surface. The bottom of the slab was passivated with pseu-

dohydrogen atoms of nuclear charge $+4/3$ and $+2/3$ in order to achieve well-converged results. This is our so-called “standard setup” which has been previously carefully constructed⁹ by performing extensive tests on the convergence of surface energies as well as hydrogen and water adsorption energies, with respect to both the number of relaxed outermost trilayers and the thickness of the slab itself (see tables and graphs in⁹ for detailed comparisons). The system size employed in our calculations, corresponding to 208 atoms for the stoichiometric slab, belongs to the largest systems used so far in order to model the surface, in particular when it comes to performing *ab initio* molecular dynamics. In order to further check the convergence we optimized two five trilayer slabs (one with an empty surface O vacancy and one with an Au adatom at this vacancy) and confirmed that the resulting spin density and excess charge localization is the same as reported herein for our “standard setup”.

The gradient-corrected Perdew-Burke-Ernzerhof functional (PBE)⁸¹ was employed to describe semilocally the exchange-correlation effects. The spin-polarized Kohn-Sham equations were solved in the plane wave / pseudopotential framework using Vanderbilt’s ultrasoft pseudopotentials⁸² with a cutoff of 25 Ry using the Γ -point. The Ti pseudopotential was constructed from an ionic $3d^4 4s^2$ configuration and the $3s$ and $3p$ semicore electrons were treated as full valence states. It is well established that adding a Hubbard U term acting on the Ti- $3d$ orbitals greatly improves the quality of LDA or GGAs in describing the electronic structure of both oxidized and reduced titania surfaces^{13,79,80,83–88}. Following our previous work¹³, we used a self-consistent linear response formalism^{89,90} to compute the Hubbard term, which turns out to be $U = 4.2$ eV for this particular setup; the occupations of the d orbitals were calculated using atomic-like wave function projectors. It will not have escaped attention that our value of the U parameter is larger than that recently derived by Mattioli et al.⁹¹ (i.e. $U = 3.25$ eV). This can be attributed to the different d -orbitals used as projectors for the integration of the d -orbital occupation numbers. The U value of 3.25 eV obtained in⁹¹ was derived using the d -orbital of the neutral Ti atom as a projector, whereas our value, $U = 4.20$ eV, is computed by using Ti^{+1} as a reference, which in our opinion more closely resembles the charge state of Ti in the $\text{TiO}_2(110)$ surface. At this point it should be noted that we also obtained $U = 3.20$ eV when using the d -orbital of the neutral Ti atom as the projector instead, which is in agreement with the U value reported in⁹¹. Similarly, performing the calculations of FeO Pickett et al.⁹² showed that the calculated Hubbard energy strongly depends on the choice of d -orbital. Using the d -orbital of the neutral Fe atom they obtained $U = 4.6$ eV whereas using the Fe^{+2} dication yields a substantially larger value of $U = 7.8$ eV. This is a well-known and still poorly understood shortcoming of the U parameter derivation procedures that use atomic-like d -orbitals as projectors for the integration of the occupations of the

d -orbitals in solids, which, in turn, is an input for the computation of the Hubbard correction to LDA/GGA density functionals⁸⁹. The static optimizations for the different $\text{TiO}_2(110)$ surface structures were carried out using the **Quantum Espresso**⁹³ code. All structures were relaxed by minimizing the atomic forces, where convergence was assumed to have been achieved when the maximum component of the residual forces on the ions was less than 0.02 eV/Å. Here, only the lowest trilayer atoms were constrained to their equilibrium positions while all other atoms were free to move during optimization. All *ab initio* molecular dynamics (AIMD) simulations⁹⁴ were carried out using the same spin-polarized PBE+ U approach, together with the Car-Parrinello propagation scheme,⁹⁵ using a fictitious electron mass of 700 a.u. and a time step of 0.145 fs. Our in-house modified version of the CPMD⁹⁶ code was used for this purpose.

The adsorption energy $E_{\text{ads}}^{\text{H}}$ per H atom on the stoichiometric $\text{TiO}_2(110)$ surface is computed from

$$E_{\text{ads}}^{\text{H}} = \frac{1}{N_{\text{H}}} \left[E_{\text{tot}}^{\text{H-ads}}(N_{\text{H}}) - \left(E_{\text{tot}}^{\text{slab-TiO}_2} + \frac{N_{\text{H}}}{2} E_{\text{tot}}^{\text{H}_2} \right) \right], \quad (1)$$

where $E_{\text{tot}}^{\text{H-ads}}(N_{\text{H}})$ is the total energy of the slab saturated with N_{H} H adatoms; here $E_{\text{tot}}^{\text{slab-TiO}_2}$ is the energy of the stoichiometric slab, which we take as a reference, and $E_{\text{tot}}^{\text{H}_2}$ is the energy of a H_2 molecule. When dealing with CO, H_2O , and Au, the adsorption energies on stoichiometric and reduced $\text{TiO}_2(110)$ surfaces were calculated according to

$$E_{\text{ads}} = E_{\text{tot}}^{\text{sub+X}} - (E_{\text{tot}}^{\text{sub}} + E_{\text{tot}}^{\text{X}}), \quad (2)$$

where $E_{\text{tot}}^{\text{sub+X}}$, $E_{\text{tot}}^{\text{sub}}$, and $E_{\text{tot}}^{\text{X}}$ are the total energies of the combined system, the (Au/) $\text{TiO}_2(110)$ surface in a certain oxidation state, and the isolated X adsorbate, respectively. The adsorption energies were calculated with and without inclusion of the Hubbard U term correction to the standard density functional, i.e. using the plain PBE and the PBE+ U approaches. The O-vacancy formation energy was calculated using

$$E_{\text{V}}^{\text{O}} = E_{\text{tot}}^{\text{O-V}} - \left(E_{\text{tot}}^{\text{slab-TiO}_2} - \frac{1}{2} E_{\text{tot}}^{\text{O}_2} \right), \quad (3)$$

where $E_{\text{slab}}^{\text{O-V}}$ and $\frac{1}{2} E_{\text{tot}}^{\text{O}_2}$ represent the total energy of the defective system and of the O atom, respectively. Because (semi)local functionals are known to overbind molecular O_2 , the total energy of the O atom was adjusted in the manner of our previous work⁹.

In order to analyze the thermodynamic stability of our different structures in the presence of H adatoms, we employ the formalism of approximate *ab initio* thermodynamics^{97–101} by assuming that the surfaces can exchange H atoms with a surrounding gas phase. Assuming thermodynamic equilibrium, the most stable surface composition at a given temperature T and pressure p is given by the minimum of the surface Gibbs free energy. Since

we are only interested in the relative stabilities of surface structures, we directly compute the differences in the surface Gibbs free energies $\Delta G_{\text{ads}}(T, p)$ between the defective and the ideal surface according to

$$\Delta G_{\text{ads}}(T, p) = \frac{1}{A} \left[E_{\text{tot}}^{\text{H-ads}}(N_{\text{H}}) - \left(E_{\text{tot}}^{\text{slab-TiO}_2} + \Delta N_{\text{H}} \mu_{\text{H}}(T, p) \right) \right], \quad (4)$$

where A is the surface area, ΔN_{H} is the difference in the number of H atoms between the two surfaces, and $\mu_{\text{H}}(T, p)$ is the chemical potential representing the Gibbs free energy of the gas phase with which the H atoms are exchanged. Assuming that all differences in entropy and volume contributions in $\Delta G_{\text{ads}}(T, p)$ are negligible, the Gibbs free energies are approximated by their respective total energies of our DFT slab calculations as usual⁹⁹⁻¹⁰¹. The upper bound for the chemical potential $\mu_{\text{H}}(T, p)$ is given by the total energy of its most stable elemental phase⁹⁸, that is, molecular hydrogen ($\frac{1}{2}E_{\text{tot}}^{\text{H}_2}$). This upper bound is taken as the zero of our energy scale by using $\Delta \mu_{\text{H}} = \mu_{\text{H}}(T, p) - \frac{1}{2}E_{\text{tot}}^{\text{H}_2}$.

In a similar way, the effect of temperature and pressure on the relative stability of the Au/TiO₂(110) surface structures is studied by employing the formalism of approximate *ab initio* thermodynamics⁹⁷⁻¹⁰¹. The free energy of formation of the Au/TiO₂(110) surface structures $\Delta_{\text{ads}}G(T, p)$ is assumed to depend on the temperature and pressure only via the oxygen chemical potential $\mu_{\text{O}}(T, p)$ given by

$$\mu_{\text{O}}(T, p) = \mu_{\text{O}}(T, p^0) + \frac{1}{2}kT \ln \left(\frac{p}{p^0} \right). \quad (5)$$

Equation (5) represents the thermodynamics reservoir of the O₂ environment that is in contact with the surface under consideration. The free energy differences will be calculated as a function of $\Delta \mu_{\text{O}}(T, P) = \mu_{\text{O}}(T, p) - \mu_{\text{O}}(T = 0 \text{ K}, p^0)$, corresponding to changes of the oxygen chemical potential with respect to a zero reference state. The latter is set to the total energy of the O atom at $T = 0 \text{ K}$, $\mu_{\text{O}}(T = 0 \text{ K}, p^0) = 1/2E_{\text{tot}}^{\text{O}_2} = 0$. Assuming thermodynamic equilibrium of the surfaces with an O₂ gas phase, the chemical potential can be converted into a pressure scale for different temperatures by using experimental thermochemical reference data or by applying the ideal gas equation⁹⁹⁻¹⁰¹. Vibrational and rotational entropic contributions to $\mu_{\text{O}}(T, p)$ are included by means of thermodynamic tables as described in Ref. 99. Under these assumptions and neglecting entropic contributions of the solids involved, the free energy of formation as a function of pressure and temperature assumes the expression

$$\Delta G_{\text{ads}}(T, p) = \frac{1}{A} [E_{\text{tot}}^{\text{sub+X}} - E_{\text{tot}}^{\text{slab-TiO}_2} + N_{\text{O}}^{\text{v}} \mu_{\text{O}}(T, p) + N_{\text{Ti}}^{\text{v}} [E_{\text{TiO}_2}^{\text{bulk}} - 2\mu_{\text{O}}(T, p)] - \mu_{\text{Au}}], \quad (6)$$

where $E_{\text{TiO}_2}^{\text{bulk}}$ is the energy of a formula unit of the TiO₂ bulk phase. The quantities N_{O}^{v} and N_{Ti}^{v} represent the number of O or Ti vacancies that are present in the structure under consideration. Therefore, the energy cost for the formation of surface defects is taken into account in Eq. (6) via the chemical potential of O atoms and of bulk TiO₂. Finally, the chemical potential of Au, μ_{Au} , is set to be the total energy per atom of the bulk Au crystal. The upper bound for the chemical potential μ_{O} is given by the total energy of its most stable elemental phase, that is, molecular oxygen ($\frac{1}{2}E_{\text{tot}}^{\text{O}_2}$). This upper bound is used to define $\Delta \mu_{\text{O}}(T, P) = \mu_{\text{O}} - \frac{1}{2}E_{\text{tot}}^{\text{O}_2}$. A lower bound for $\Delta \mu_{\text{O}}$ is given by minus half of the formation energy of bulk TiO₂, i.e. $E_{\text{f}}^{\text{TiO}_2} = E_{\text{bulk}}^{\text{Ti}} + E_{\text{tot}}^{\text{O}_2} - E_{\text{bulk}}^{\text{TiO}_2}$, for which we have taken the theoretical value of 4.8 eV from our PBE calculations; here $E_{\text{bulk}}^{\text{TiO}_2}$ and $E_{\text{bulk}}^{\text{Ti}}$ are the energies of one bulk unit cell of TiO₂ and metallic Ti, respectively^{99,100}.

Finally, the bonding charge density has been evaluated using the expression

$$\Delta \rho(\vec{r}) = \rho_{\text{sub+X}} - (\rho_{\text{sub}} + \rho_{\text{X}}) \quad (7)$$

where the ρ 's are the respective valence electronic charge densities at position \vec{r} in space.

III. SMALL MOLECULES ON TITANIA: REFERENCE CALCULATIONS USING PBE+U

Computationally efficient implementations of DFT based on local/semilocal LDA/GGA density functionals predict rather delocalized defect levels for excess electrons in the case of reduced transition metal oxides in general, and for titania in particular. Thus, more sophisticated techniques such as hybrid functionals or GGA+U approaches are necessary to properly account for the strong correlation effects of these *d*-electrons, resulting in localization of the excess charge on *3d*-orbitals of reduced Ti atoms. However, before using PBE+U to investigate the properties of gold on titania, it is necessary to confirm that this approach does not destroy the agreement between previously reported plain PBE results (mainly optimized structures and relative energies) and experimental observations. The purpose of this section is therefore twofold: first, to validate the PBE+U approach using a test set that probes the physics and chemistry of titania surfaces interacting with adspecies relevant to heterogeneous catalysis; and, second, to check how PBE+U performs compared to plain PBE investigations for the very same systems. Thus, the interaction of H, H₂O, and CO with the TiO₂(110) substrate is investigated in the following section using the PBE+U approach where a large set of both experimental and previous theoretical data are available.

Many theoretical and experimental studies have been devoted to understanding the interaction between hydrogen atoms^{9,15-18,102} or water^{9,10,19-36} and the TiO₂(110) surface. In experiments, hydrogen atoms, when adsorbed

on $\text{TiO}_2(110)$, stick to the bridging oxygens and a maximum surface saturation limit of ~ 0.7 ML is observed¹⁸. These findings have been confirmed on purely theoretical grounds within the framework of standard GGA calculations using the PBE functional⁹. In-depth *ab initio* thermodynamics considerations reveal a maximum saturation level of hydrogen on this oxide surface of about 60–70%, in excellent agreement with the above-mentioned experimental observations. Adsorption of hydrogen on the stoichiometric surface results in its reduction by introducing one electron per adsorbed H atom into the substrate.

We first consider the interaction of H with the stoichiometric $\text{TiO}_2(110)$ surface. The hydroxylated surface has been investigated for a wide range of H coverages using both PBE+U and PBE. In agreement with both plain PBE calculations and experimental results, we find that H atoms preferentially adsorb on top of surface O_b atoms of the stoichiometric titania surface, leading to the formation of OH groups with O–H bond lengths of ~ 1 Å. In addition, our PBE+U calculations predict that one electron per H atom adsorbed on the surface is transferred to the substrate, leading to the formation of Ti^{3+} ions (see Table I). The newly-formed OH groups are found to be tilted by about 20–50° in opposite $[1\bar{1}0]$ directions, as previously reported. The PBE and PBE+U values of the adsorption energies $E_{\text{ads}}^{\text{H}}$ per H atom at different coverages are reported in Table I. The ground state configuration of the fully hydroxylated titania surface yields (2×1) symmetry, but at room temperature OH groups will be fully disordered with respect to their axes because of the tiny barrier that must be overcome in order to flip their orientation.

At all coverages, the PBE+U adsorption energies are found to be significantly lower, by about -0.3 to -0.6 eV, compared to the PBE data in Table I. However, the same stability trend obtained by employing the PBE+U functional is obtained using the standard PBE functional, i.e. a decrease of the adsorption energy with increasing coverage. Nevertheless, even at full monolayer coverage, the adsorption energy per atom is still significant and negative when using PBE+U, whereas it is close to zero according to PBE. Clearly, such total energy considerations need to be supplemented with *ab initio* thermodynamics in order to check the thermodynamic stability of the surface at different saturation levels. The results are summarized in terms of the surface free energy diagram in Fig. 1. Both PBE+U and PBE predict that the fully hydrogenated surface will be thermodynamically unstable at all accessible hydrogen partial pressures. PBE+U and PBE also agree in that saturation of this surface by hydrogen is reached at a coverage on the order of 70%. Thus, the previous PBE predictions⁹ and agreement with experimental observations¹⁸ upon hydroxylating $\text{TiO}_2(110)$ are qualitatively confirmed. (for reasoning, see the detailed conceptual discussion in Ref. 9). However, significant strengthening of the adsorption and shifts in the surface phase diagram are observed when using PBE+U, thus localizing the excess charges upon

TABLE I: Adsorption energies E_{ads} (in eV) per H atom for adsorption of hydrogen at different coverages as indicated. In the second column the number of reduced Ti^{3+} ions which are present in the substrate is reported.

| Configuration | $E_{\text{ads}}(\text{PBE+U})$ | Ti^{3+} | $E_{\text{ads}}(\text{PBE})$ |
|---------------|--------------------------------|------------------|------------------------------|
| 1H | -0.91 | 1 | -0.56 |
| 2H | -0.86 | 2 | -0.40 |
| 4H | -0.77 | 4 | -0.24 |
| 6H | -0.68 | 6 | -0.15 |
| 8H | -0.37 | 8 | -0.04 |

introducing the Hubbard correction.

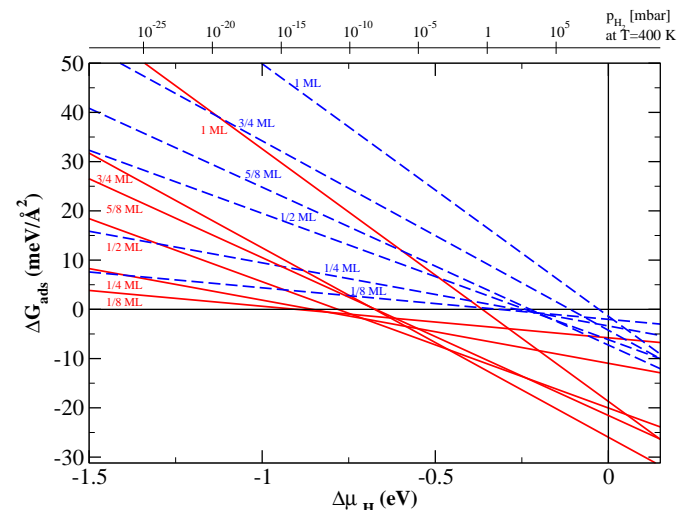


FIG. 1: Free energy $\Delta G_{\text{ads}}(T, p)$ for H adsorption on $\text{TiO}_2(110)$ stoichiometric surfaces with different hydrogen coverages as a function of the hydrogen chemical potential $\Delta\mu_{\text{H}}$. Conversion to hydrogen partial pressures p_{H_2} (upper axis) has been carried out at $T = 400$ K (see text). The red and blue lines represent the PBE+U and PBE results, respectively.

It is well-known that the investigated surface contains a significant number of oxygen vacancies ($\sim 5\%$), not just in ill-defined industrial situations, but even under well-controlled experimental conditions.² Therefore, the investigation of the adsorption of water molecules on the reduced $\text{TiO}_2(110)$ surface is of great importance in the frame of addressing the fundamental issue of dissociative *versus* molecular adsorption modes^{9,10,19,33}. We thus consider the interaction between H_2O and the TiO_2 surface. We have performed systematic PBE+U and PBE calculations of H_2O adsorbed on the reduced TiO_2 surface, considering a titania surface containing a single V_O vacancy; this greatly extends our recent comprehensive work⁹ concerning water on the stoichiometric surface using plain PBE.

The specific adsorption configurations for a water molecule on the reduced surface, which we consider in

this investigation, are compiled in Fig. 2, and the corresponding adsorption energies are collected in Table II. The Ti_{5c} surface sites are labeled in relation to the V_O vacancy, where site Ti0 denotes a nearest-neighbor Ti_{5c} atom and sites Ti1 and Ti2 are the second and third nearest-neighbour Ti_{5c} sites parallel to the O_b row containing the V_O site; see panel (a) of Fig. 2. In agreement with experimental data, we find that on the reduced surface, H_2O molecules prefer to dissociatively adsorb at V_O vacancy sites, leading to a configuration with two surface OH groups as shown in panel (b) of Fig. 2. We therefore end up with a stoichiometric titania surface with two H atoms adsorbed on two surface O_b atoms. Once the water molecule dissociates at the oxygen defect through proton transfer to an adjacent O_b atom, the PBE+U (PBE) adsorption energy is -1.61 eV (-1.18 eV). A projected PDOS analysis reveals that upon dissociation of water at the V_O site, two second-layer Ti^{3+} ions are present in the substrate. This value of E_{ads} is ~ 0.4 eV lower than the corresponding plain PBE value and previously reported values,^{35,36,103} which are between -0.94 and -1.1 eV. The energy value deduced from a water desorption peak at 520 K in TDS experiments¹⁰⁴ using the simple Redhead formula¹⁰⁵ is about -1.4 eV, which is between the PBE+U and PBE values. However, the estimation of desorption energies using the Redhead formula can be biased by as much as 25%, which implies that both values must be considered to be consistent with experiment. We now turn our attention to the adsorption and dissociation of water at Ti_{5c} sites next to V_O . We anticipate that, as observed in the case of H_2O dissociatively adsorbed at the V_O site, the interaction between water and the Ti_{5c} sites does not further reduce the metal oxide support. All PBE+U calculations predict the presence of two reduced Ti^{3+} ions before and after the adsorption of H_2O at Ti_{5c} sites. Water molecules can be adsorbed either dissociatively (labeled as “D”) or molecularly (“M”) at the various Ti_{5c} sites (i.e. Ti0, Ti1, and Ti2) next to V_O (see Fig. 2). When H_2O dissociates at a Ti_{5c} site, the resulting configuration contains an OH group bonded to a Ti_{5c} atom and an H atom bonded to a nearest-neighbor O atom of the Ti_{5c} in the $[1\bar{1}0]$ direction. We have considered two different topologies: first, where the H atom coming from the dissociated water molecule binds to an O atom belonging to the O_b row in which the V_O vacancy site is present (labeled configuration “A”); and second, with the H atom bonded to O atoms belonging to an adjacent O_b row parallel to the O_b row that hosts V_O (configuration “B”). See Table II for the corresponding adsorption energies.

Our PBE+U and PBE calculations suggest that, in the presence of an oxygen vacancy, water molecules adsorb dissociatively or molecularly at Ti_{5c} sites with E_{ads} in the range of -0.45 to -0.92 eV. Once the water molecule dissociates at a Ti_{5c} site, it forms a pair of terminal hydroxyls. Therefore, in the dissociative case, we always end up with an OH group bonded to a Ti_{5c} site and a protonic H atom transferred to an adjacent O_b atom,

TABLE II: Adsorption energies E_{ads} (in eV) in the case of adsorption of water on the reduced surface for PBE+U and plain PBE reported in parentheses; see Fig. 2 for labeling.

| configuration | site Ti0 | site Ti1 | site Ti2 |
|--------------------------|----------------|----------------|----------------|
| DA | 2.27 (1.58) | -0.71 (-0.81) | -0.45 (-0.48) |
| MA | -0.77 (-0.79) | -0.73 (-0.76) | -0.72 (-0.72) |
| DB | -0.87 (-0.89) | -0.92 (-0.95) | -0.89 (-0.90) |
| MB | -0.77 (-0.80) | -0.83 (-0.81) | -0.84 (-0.82) |
| $\text{H}_2\text{O}@V_O$ | -1.61 (-1.18) | | |

the O_b atom belonging either to the O_b row that contains V_O , or to the adjacent one that contains no oxygen vacancy. As shown in Table II the most stable dissociative configurations are those with the protonic H atom transferred to an O_b atom of an O_b row parallel to the row featuring the V_O site (configurations denoted “DB” in Table II and Fig. 2). The PBE+U/PBE calculations show that protons prefer to bind to O_b atoms belonging to an O_b row in absence of V_O sites, with E_{ads} ranging from -0.87 to -0.95 eV.

Otherwise, if we consider the case where, after water dissociation at a Ti_{5c} site, a proton transfers to an O_b atom belonging to an O_b row that includes a V_O site (configurations denoted “DA” in Table II and Fig. 2), our calculations provide adsorption energies in the range of -0.45 to -0.71 eV; the same trend is observed with or without the inclusion of a Hubbard U term in the calculations. We note that the structure with an OH group adsorbed at a Ti_{5c} site and an H placed right at the V_O vacancy is unstable; the adsorption energy of this configuration E_{ads} is positive by 2.27 eV.

Our results show that on the reduced $\text{TiO}_2(110)$ surface, water prefers to adsorb dissociatively onto Ti_{5c} sites. Once water molecules are molecularly adsorbed on the reduced surface, the binding energy of the surface is about 0.1 eV higher than it is when water is dissociated on the same substrate. These findings are in agreement with previous studies of H_2O interaction with the stoichiometric $\text{TiO}_2(110)$ surface. However, as shown based on carefully converged calculations⁹, molecular and dissociated configurations become essentially energetically degenerate at very low coverages, which explains why some studies favor molecular adsorption whereas others yield the dissociated state as the lowest energy configuration in this regime¹⁰. Most experimental works, except a recent one¹⁰⁶ claiming mixed adsorption, indicate molecular adsorption only. This gives rise to the well-known discrepancy between theoretical predictions and experimental results in providing a consistent and comprehensive picture of water adsorption on titanium dioxide surfaces, in particular at low coverages.

Last but not least, we focus on the interaction between CO and the $\text{TiO}_2(110)$ surface. It is well known that, on the stoichiometric $\text{TiO}_2(110)$ surface, the CO molecule adsorbs onto Ti_{5c} sites, thus forming Ti-C bonds. Because van der Waals dispersion interactions and non-

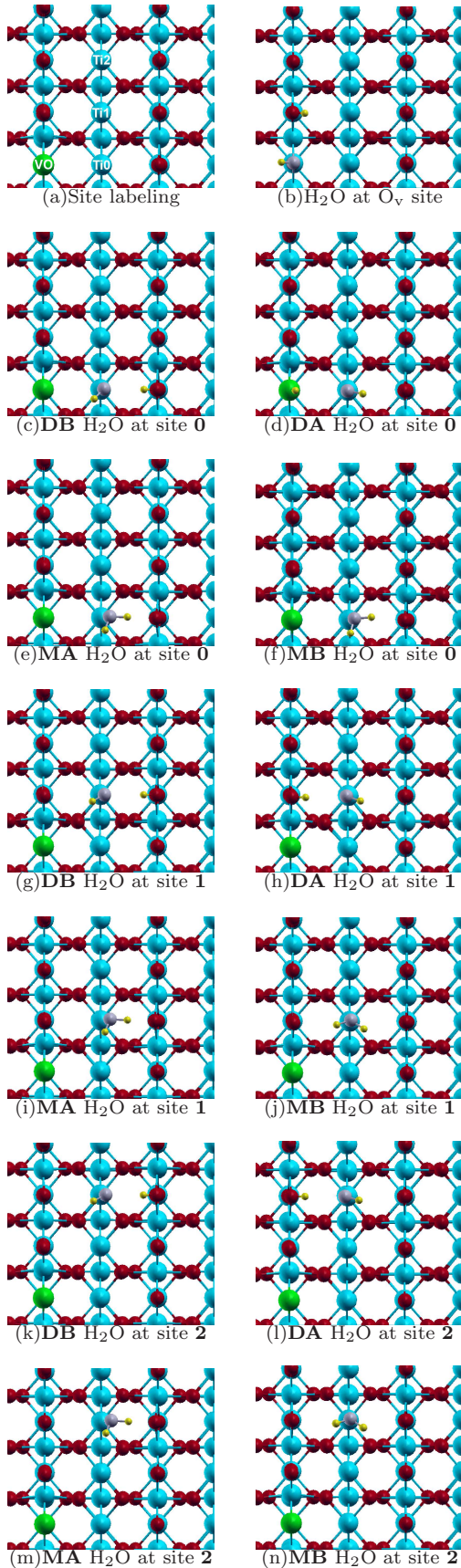


FIG. 2: Ball and stick models of relevant configurations (see text) for an H_2O molecule adsorbed either molecularly (“M”) or dissociatively (“D”) in two configurations (“A” and “B”) on $\text{TiO}_2(110)$ surfaces (top view) at V_O , Ti_0 , Ti_1 , and Ti_2 sites (see panel (a) for site labeling) obtained using the PBE+U approach. Red, blue, violet, and yellow spheres are substrate O, Ti, water O, and H atoms, respectively, and the oxygen vacancy site V_O is highlighted using a green sphere.

TABLE III: Adsorption energies E_ads (in eV) of a CO molecule adsorbed on the reduced rutile $\text{TiO}_2(110)$ surface at different sites, labeled according to Fig. 3. In the second column, the number of reduced Ti^{3+} ions present in the substrate is reported.

| Configuration | $E_\text{ads}(\text{PBE}+\text{U})$ | Ti^{3+} | $E_\text{ads}(\text{PBE})$ |
|-------------------------|-------------------------------------|------------------|----------------------------|
| CO@ V_O | -0.32 | 2 | -0.29 |
| CO@ Ti_0 | -0.22 | 2 | -0.28 |
| CO@ Ti_1 | -0.29 | 2 | -0.30 |
| CO@ Ti_2 | -0.33 | 2 | -0.29 |

local electron correlations significantly influence this type of bonding, we have previously investigated the interaction of CO with the stoichiometric $\text{TiO}_2(110)$ surface using a combination of DFT and post Hartree-Fock (“SCS-MP2”) methods³⁹. The CO binding energy has been found to vary significantly with coverage and increases upon reaching the saturation limit. The SCS-MP2 E_ads computed values are -0.20 eV for the full saturated surface and -0.36 eV for a single CO molecule adsorbed on the surface. The PBE adsorption energy of a single CO molecule, -0.32 eV, is close to the SCS-MP2 value of -0.36 eV, and both energies are in accord with the experimental value obtained by means of thermal desorption spectroscopy. This demonstrates that PBE as such is able to describe the interaction of CO with the ideal (110) rutile surface in the limit of low coverages, which remains unaltered when using PBE+U, which gives -0.31 eV for the adsorption energy.

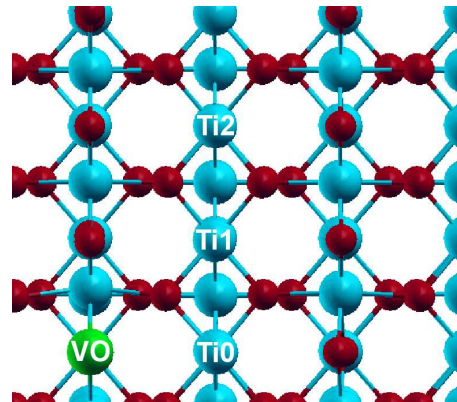


FIG. 3: Ball and stick model of the $\text{TiO}_2(110)$ surface (top view), with site labeling. Red and blue spheres are O and Ti atoms, respectively, and the oxygen vacancy site, V_O , within the bridging oxygen row, O_b , is highlighted using a green sphere.

We now turn our attention to CO adsorbed onto the O vacancy site, V_O , as well as on the fivefold coordinated surface sites, $\text{Ti}_{5\text{c}}$, at various distances from the vacancy. Note that the $\text{Ti}_{5\text{c}}$ site belongs to the Ti row next to the bridging O_b row containing V_O (see Fig. 3).

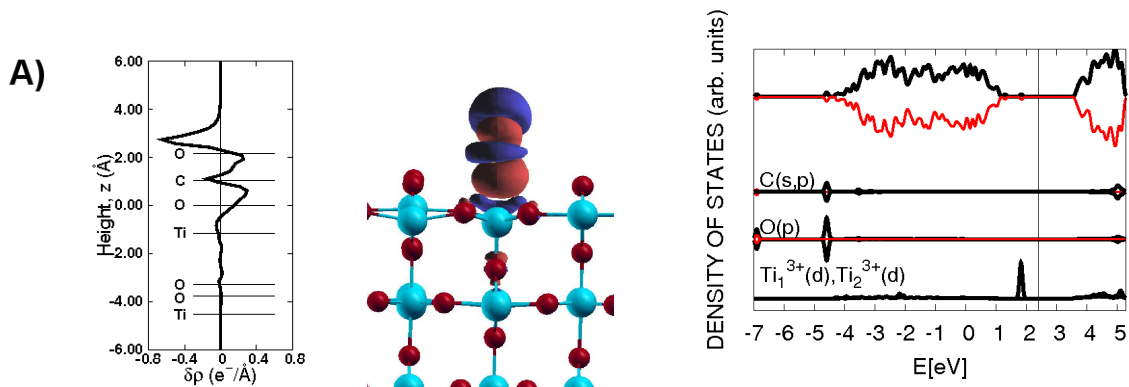


FIG. 4: Electronic structure analyses (based on the PBE+U approach) of molecular CO adsorbed on the reduced $\text{TiO}_2(110)$ surface at the Ti2 site with respect to the oxygen vacancy, V_{O} , located in the row of bridging oxygens, O_{b} (see Fig. 3 and Table III). The left panel represents the bonding charge $\delta\rho(z)$ integrated in planes perpendicular to the surface and plotted as a function of the height from the surface. The central panel displays the bonding charge $\Delta\rho(\vec{r})$ at an iso-value of $\pm 0.06 |e|/\text{\AA}^3$ where electron accumulation and depletion are represented by red and blue areas, respectively. The right panel shows the total DOS and atom-resolved projected DOS (PDOS) as indicated; here, energy values are with respect to the Fermi level, which is marked by a solid vertical line.

In each case, the CO molecule is placed perpendicular to the substrate, with the carbon atom pointing toward the surface. All the structures are fully relaxed according to our aforementioned convergence criterion. The computed adsorption energies (E_{ads}) are compiled in Table III. Interestingly, we do not see a significant variation in the adsorption energies computed for different structures. The PBE+U (PBE) adsorption energy for the CO molecule adsorbed at the surface O_{b} vacancy site is -0.32 eV (-0.29 eV). CO adsorption at sites Ti1 and Ti2 results in adsorption energies of -0.29 eV (-0.30 eV) and -0.33 eV (-0.29 eV), respectively (see Fig. 3 for site labeling scheme). The computed values of E_{ads} are in qualitative agreement with previous studies^{107,108}. We note that these values are close to those obtained when CO is adsorbed at the V_{O} vacancy site (-0.32 eV) and on the stoichiometric surface³⁹, i.e. -0.31 eV (-0.32 eV) for PBE+U (PBE). When adsorbed at site Ti0, the adsorption energy of the CO molecule, computed with PBE+U, results in a distinctly higher value for E_{ads} of -0.22 eV in agreement with Ref. 108, while the corresponding PBE value is -0.28 eV, comparable to the adsorption at sites Ti1 and Ti2. Our PBE+U results therefore confirm previous findings that CO molecules weakly interact with the reduced $\text{TiO}_2(110)$ oxide surface, E_{ads} being of the order of about -0.3 eV (see Refs. 39,107,108). The calculations indicate that CO adsorbs at both V_{O} vacancies and $\text{Ti}_{5\text{c}}$ sites, but while PBE calculations give similar energy values for CO adsorption at V_{O} vacancies and at Ti0, Ti1, and Ti2 sites, the inclusion of a Hubbard U term suggests that the adsorption of CO at Ti0 sites, the sites facing the V_{O} vacancy, is discouraged. In this case, the adsorption energy E_{ads} is found to be ~ 0.1 eV higher when compared to the adsorption energy values at sites Ti1 and Ti2. Upon CO adsorption on the reduced sur-

face, the charge redistribution that results from attaching the molecule does not further reduce the oxide support: the PBE+U calculations yield two Ti^{3+} ions before and after adsorption, which results in an insignificant change in the adsorption energies when switching from PBE to PBE+U calculations. This behavior is confirmed by the computed electronic density of states (DOS). In Fig. 4, we depict the electronic DOS and the bonding charge density $\Delta\rho$ of the structure where a CO molecule is attached at the $\text{Ti}_{5\text{c}}$ site (labeled site Ti2 in Fig. 3). The electronic DOS features a peak in the band gap below the Fermi level. The projected DOS (PDOS) analysis reveals that this filled gap state is related to the charge localized on two Ti-3d orbitals that yield the two reduced Ti^{3+} sites. We conclude therefore that the binding of a CO molecule does not induce a significant charge rearrangement at the CO/oxide contact site. However, as we will show, the catalytic activity of the $\text{TiO}_2(110)$ substrate for efficient CO oxidation is improved by supported and dispersed Au adatoms on this substrate.

In conclusion, this detailed assessment convincingly demonstrates that although similar trends are observed in the adsorption energies with or without the inclusion of a Hubbard U correction, the PBE+U method is seen to significantly *improve the description of the electronic structure whenever reduction occurs*. In particular, the localization of excess charge on the titania substrate induced by O vacancies (F -centers) or upon H atom adsorption on bridging O atoms (hydroxylation), is correctly predicted by the PBE+U approach. Clearly, an adequate description of the electronic structure of such $\text{TiO}_2(110)$ surfaces is crucial when dealing with metal-promoted oxide surfaces in the realm of catalysis.

IV. GOLD-PROMOTED TITANIA: ELECTRONIC STRUCTURE, DYNAMICS, AND THERMODYNAMICS FROM PBE+U

A. Au adatom adsorption on the stoichiometric TiO₂(110) surface

Having shown that the PBE+U formalism performs well for a set of reference calculations on the adsorption of H, H₂O, and CO on stoichiometric and reduced TiO₂(110) surfaces, and that it significantly improves the description of reduced titania surfaces, we now progress to investigating the interactions between gold and TiO₂(110) surfaces. The adsorption or substitution of gold induces strong charge rearrangements at the Au/oxide contact, which affects the electronic structure. Of particular interest in the realms of metal/support interactions and heterogeneous catalysis is the oxidation state of Au adatoms, which is determined by the site where the metal atom is adsorbed, as well as by the stoichiometry of the supporting oxide. As in previous GGA studies^{7,64,66,69}, two stable adsorption sites of a single Au adatom on the stoichiometric TiO₂(110) surface have been identified, the two structures differing by only ~ 0.1 eV in energy. The most stable adsorption site for an Au adatom deposited on this titania surface is a bridge site between an O_b and a Ti_{5c} atom as depicted in the central panel of Fig. 5 (B). The computed PBE+U (PBE) adsorption energy and the Au–O / Au–Ti bond lengths are -0.58 eV (-0.41 eV) and 2.30 (2.39) / 2.79 Å (2.88 Å) respectively, in agreement with previous studies^{7,12,64,66,69} based on standard GGA calculations; see Table IV for a summary.

The bonding charge density analysis reveals that $0.11 |e|$ are transferred from the metal atom to the oxide substrate, thus indicating a very weak oxidation of Au. The excess charge in the substrate is mostly localized around the O_b bonded to the Au adatom. This value of the charge transfer has been obtained by integrating the bonding charge density on planes parallel to the surface from the center of the vacuum region to the center of the O–Au–Ti bond (see left panel of Fig. 5 (B)). As demonstrated by the PDOS analysis shown in the right panel of Fig. 5 (B), in this configuration all the Ti ions belonging to the substrate preserve their formal oxidation state Ti⁴⁺.

The second identified stable site is a top site (see central panel of Fig. 5 (C)), where the Au adatom is adsorbed on top of an O_b atom. The corresponding PBE+U (PBE) adsorption energy and the Au–O bond length are -0.48 eV (-0.29 eV) and 2.00 Å (2.16 Å), akin to previous GGA studies^{64,69}. Again, a net charge transfer from metal to surface, leading to a positively charged Au^{δ+} ion, is observed. In this case, however, the magnitude of the charge transfer, $0.35 |e|$, is more significant, i.e. three times larger than in the previous case. The excess charge in the substrate is now mostly localized around the surface O_b atom bound to the Au^{δ+} and a second-

TABLE IV: Adsorption energies E_{ads} (in eV) of Au and CO species on stoichiometric and reduced rutile TiO₂(110) surfaces and on the Au/TiO₂ metal/support system; see text for labeling. In the second column, the number of reduced Ti³⁺ ions present in the substrate is reported.

| | $E_{\text{ads}}(\text{PBE+U})$ | Ti ³⁺ | $E_{\text{ads}}(\text{PBE})$ |
|------------------------------------|--------------------------------|------------------|------------------------------|
| Au@O(bridge) | -0.58 | 0 | -0.41 |
| Au@O(top) | -0.48 | 1 | -0.29 |
| Au@V _O | -1.54 | 1 | -1.57 |
| Au ₂ @V _O | -1.17 | 2 | -1.19 |
| Au@V _{Ti5c} | -6.38 | 0 | -6.21 |
| CO@Au@O(bridge) | -2.27 | 1 | -2.17 |
| CO@Au@O(top) | -2.66 | 1 | -2.33 |
| CO-Au@V _O | -0.41 | 1 | -0.32 |
| CO-Au ₂ @V _O | -1.22 | 2 | -1.00 |

layer Ti ion which reduces Ti⁴⁺ \rightarrow Ti³⁺ (see Fig. 5 (C)). The reduced Ti³⁺ ion is located at a site adjacent to the Au^{δ+} adatom in the second subsurface layer under the Ti_{5c}. These findings are corroborated by the computed DOS plotted in Fig. 5 (C), which displays two features in the band gap. The projected DOS analysis reveals that the filled state below the Fermi level and closest to the valence band results from the charge transferred from the metal to the substrate being localized on a second-layer reduced Ti³⁺ atom. The unoccupied level closest to the conduction band is instead related to the Au–O bonding. The 6s levels of Au are partially empty and are located above the Fermi level, leading to the Au oxidation.

In summary, the PBE+U calculations predict two lowest-energy configurations for Au adsorption on the stoichiometric TiO₂(110) surface: a bridge site with the Au adatom adsorbed between O_b and Ti_{5c} atoms and a top site with the Au adatom adsorbed on top of an O_b atom. Once adsorbed at the bridge site, a very weak oxidation of the Au adatom is observed. On the other hand, the adsorption process of Au on top of an O_b atom induces a net charge transfer from the adsorbate to the substrate, leading to the formation of a distinctly positively charged Au^{δ+} species where about a third of an electron is transferred from the metal atom to the oxide substrate. A qualitatively similar scenario has been observed in recent studies of the related Au/CeO₂ system^{109–111}. However, unlike titania, with ceria the charge transfer involved in the adsorption of Au on the stoichiometric oxide surface always leads to the reduction of a substrate Ce ion. In addition, the fact that the excess charge δ^- , stemming from Au in the present case, localizes on a second-layer Ti ion is in line with our recent findings on reduced titania surfaces¹³.

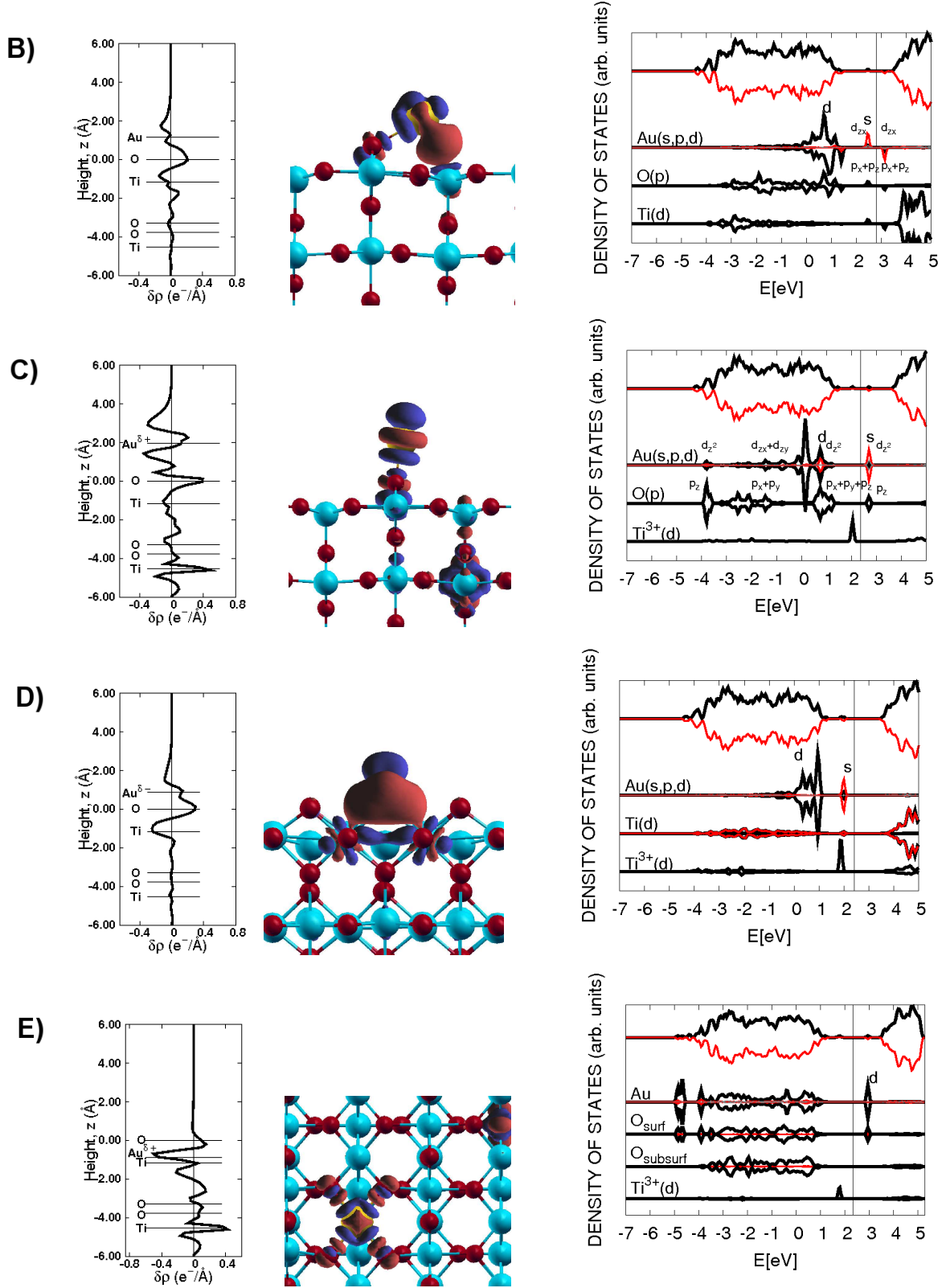


FIG. 5: Electronic structure analyses (based on the PBE+U approach) of an Au adatom (B) supported by the stoichiometric $TiO_2(110)$ surface in the bridge position, (C) supported by the stoichiometric $TiO_2(110)$ surface in the top position, (D) adsorbed on a surface V_O vacancy on the $TiO_2(110)$ surface, and (E) substituting a surface Ti_{5c} atom in the presence of a surface V_O vacancy in a bridging position on the $TiO_2(110)$ surface (see Fig. 9). Left panels represent the bonding charge $\delta\rho(z)$ integrated over planes perpendicular to the surface and plotted as a function of the height from the surface. Central panels display the bonding charge $\Delta\rho(\vec{r})$ at an isovalue of $\pm 0.06 |e|/\text{\AA}^3$ where electron accumulation and depletion are represented by red and blue areas, respectively. Right panels show the total DOS and atom resolved projected DOS (PDOS) as indicated, where energy values are with respect to the Fermi level, which is marked by a solid vertical line.

B. Au adatom diffusion on the stoichiometric TiO₂(110) surface

Several previous theoretical studies^{7,67,68} explored the PES of a single Au adatom deposited on the stoichiometric TiO₂(110) surface or adsorbed onto a V_O vacancy site using static calculations, including nudged elastic band (NEB) mappings¹¹². A key finding of these investigations is that the PES for Au migration is quite flat, with low energy barriers. This indicates that Au might diffuse rather easily on the stoichiometric surface. The estimated values of the energy barriers^{7,67,68} agree with the experimental observation of facile Au diffusion on the oxide surface even at temperatures as low as 140 K, as well as the estimates for the binding energy of 0.5 eV and small migration barriers of 0.07 eV (see Refs. 12,50).

Inspired by these findings, we decided to perform explicit dynamics using unconstrained *ab initio* molecular dynamics⁹⁴ in order to reveal the mechanism of diffusion of an Au adatom on the stoichiometric TiO₂(110) surface. In order to probe the dynamics more efficiently, the temperature of the simulations was set to $T = 900$ K using the Car-Parrinello scheme⁹⁵ to propagate the system consistently using the PBE+U functional. The selected temperature is far above ambient yet sufficiently low so as to not decompose the surface. Thus, the phonon dynamics is accelerated and the sampling of the PES is enhanced on the picosecond AIMD time scale. As starting configurations for the AIMD simulations, we employed one structure in which the Au adatom is adsorbed on top of an O_b atom (see Fig. 5 (C) and Table IV) and a second structure where it is adsorbed in a bridge position between an O_b atom and a Ti_{5c} atom (see Fig. 5 (B) and Table IV). After equilibrating the structures at 300 K for several picoseconds, the system was heated to the target temperature of 900 K for the present analysis.

Let us first consider the scenario with the Au adatom adsorbed on top of a surface O_b atom, labeled as site O1 in Fig. 6, where the diffusion path of the Au adatom on the stoichiometric TiO₂(110) surface is visualized. During the simulation, the Au adatom diffuses in the [001] direction along the row of bridging oxygen atoms, O_b. Adatom diffusion is mediated by the Au atom hopping between nearest-neighbor oxygen atoms. As demonstrated in Fig. 6, the Au adatom is originally bonded to the surface bridging O1 atom with an Au–O1 bond length of ~ 2 Å (red line); it diffuses along the O_b row and after ~ 0.75 ps reaches a configuration where it is equidistant between the O1 and O2 atoms. Then it jumps on top of the row's next atom, the O2 site, where the Au–O2 bond length is ~ 2 Å (green line). The Au diffusion proceeds along the O_b row and at about 2 ps the Au adatom is shared between O2 and the next site, O3 (blue line), until it jumps on top of O3 forming a bond of ~ 2 Å.

The charge localization and charge hopping dynamics along the adatom migration path is monitored by computing, as a function of time, the occupation matrix of each Ti $d-\alpha$ and $d-\beta$ spin orbital along the trajectory

(same analysis as in¹³). As shown in Fig. 8 the excess charge donated by the Au atom to the substrate is initially localized on the second-layer Ti2 site but transfers from there to site Ti3 on the sub-picosecond time scale (at $t \sim 0.75$ ps). As seen by comparing Fig. 8 to Fig. 6, one observes that $t \sim 0.75$ ps corresponds exactly to the jump of Au from the O1 to the O2 site. A qualitatively similar scenario happens at about 2 ps which corresponds to the next hopping event of the Au atom from site O2 to O3. Thus, the motion of the surface gold adatom along the row of bridging oxygen atoms, O_b, appears to be fully correlated with the localization and hopping dynamics of the excess charge injected into the oxide support in the second layer of Ti atoms.

This dynamical scenario is distinctly different from what has been found recently for the excess charge induced by oxygen vacancies V_O in the bridging row on the same substrate¹³. In the presence of gold adatoms, the present simulations suggest a more localized configuration for the excess electron. This localized electron appears to preferentially populate sites in the vicinity of the Au atom and to closely follow the motion of the oxidized adatom. Another interesting phenomenon observed during the simulation is the absence of excess charge on the substrate at about 1.5 ps. Computing the spin density close to $t = 1.5$ ps we observe that the charge localized at second-layer Ti sites disappears from the substrate and goes to the Au adatom, where it sits for a fraction of a picosecond before returning to the substrate and occupying the Ti3 site. As observed in our previous work¹³ the excess charge populating specific second-layer Ti sites and coming from the Au adatom adsorbed on top of O_b atoms migrates easily by phonon-assisted (thermally activated) hopping to other Ti sites.

Next we consider the situation where the Au adatom is initially adsorbed at a bridge position between an O_b atom and a Ti_{5c} atom (see Fig. 7). There it forms two bonds with the O1 and Ti1 atoms, with Au–O1 and Au–Ti1 bond lengths of ~ 2.3 Å (red line) and ~ 2.8 Å, respectively. Also in this case, the gold atom originally bonded to the O1 and Ti1 atoms is found to diffuse exclusively along the [001] direction. Now, however, the gold atom hops between pairs of nearest-neighbor O and Ti atoms. After ~ 0.8 ps, a configuration is reached in which the gold atom is equidistant between the O1 and O2 (and Ti1 and Ti2) sites before it jumps into another bridge position between the O2 (green line) and Ti2 sites. By performing static calculations, we show that Au adatoms adsorbed on bridge sites do not induce reduction of the substrate (see Fig. 5 (B)), thus all the Ti ions of the substrate preserve their 4+ oxidation state and a very weak oxidation of the Au adatom is observed. This is fully confirmed by the dynamical simulations: along the trajectory, the Ti-3*d* orbitals are found to be empty, which implies that no localization of charge on substrate Ti sites is observed.

Even at an elevated temperature of 900 K, we do not observe diffusion of the Au adatom in the [110] direction,

namely from the top of O_b atoms to bridge sites between Ti_{5c} and O_b atoms, on the timescale of picoseconds. This dynamics is consistent with previous findings^{7,67} based on static or NEB¹¹² calculations which predict a relatively high energy barrier, ~ 0.35 eV, for this process to happen compared to others. In conclusion, dynamical PBE+U simulations demonstrate that Au adatoms diffuse highly directionally on the stoichiometric rutile (110) surface. They can easily migrate either along the top of the bridging oxygen rows of the clean $TiO_2(110)$ surface or around the area between these rows from one bridging position to the next one along the [001] direction. We did not observe, on the picosecond timescale, translational motion perpendicular to this direction, e.g. from one O_b row to a neighboring row via suitable bridging positions.

C. Au adatom adsorption on the reduced $TiO_2(110)$ surface

Starting with the reduced $TiO_2(110)$ surface in the presence of an O_b surface oxygen vacancy the Au metal adatom is found to adsorb preferentially at the V_O vacancy. Such surface oxygen vacancies result in stable anchoring sites for Au adatoms, which bind at about 0.90 Å above the O vacancy site with two Ti nearest neighbors at 2.68 Å obtained from both PBE+U and PBE. The corresponding PBE+U (PBE) calculated adsorption energies of -1.54 eV (-1.57 eV) are much larger than the binding to the stoichiometric surface (see Table IV), which is consistent (-1.6 to -1.8 eV) with previous GGA calculations⁶⁸. The strong adsorption of an Au atom at the V_O site entails a strong charge rearrangement at the Au/oxide contact. In the presence of an isolated V_O vacancy, the charge neutrality of the system is maintained by the presence of two reduced Ti^{3+} ions. The bonding charge distribution (see Fig. 5 (D)) shows that, upon Au adsorption at the V_O vacancy site, the charge transfer occurs now from the reduced substrate to the supported metal atom, thus leaving a reduced surface with a single Ti^{3+} ion. This indicates that the charge transferred from the reduced substrate to the adsorbate comes from one of the two Ti^{3+} ions. As a result this process leads to the formation of a negatively charged $Au^{\delta-}$ adspecies. The analysis of the DOS (see Fig. 5 (D)) now shows that the charge transferred from the substrate to the Au atom moves toward the latter’s half-filled 6s band, which turns out to be almost completely filled. In conclusion, these calculations not only suggest a greatly increased stability of Au adatoms adsorbed onto O vacancies when compared to the stoichiometric surface as a reference, but also a very different chemical reactivity with respect to ad molecules in view of their different charge state. The resulting ramifications for CO activation will be discussed in Sec. V B.

D. Au substitutional defects on the $TiO_2(110)$ surface: $Au_xTi_{(1-x)}O_{2-\delta}$

Another reaction channel of gold interacting with titania surfaces is via the chemical exchange of Ti atoms. We studied the scenario where an Au atom substitutes a surface Ti_{5c} site, which we call “ $Au@V_{Ti_{5c}}$ ”. The presence of such an Au substitutional point defect induces a rearrangement of the neighboring atoms, leading to the formation of a distorted squared planar “ AuO_4 ” unit (see Fig. 9). In this configuration, the Au atom relaxes outward by 0.62 Å and is found to be coordinated by four surface O atoms (at about 2.0 Å). The incorporation of an Au atom into the titania surface does not yield a change in the occupation of the Ti-3d states: all Ti ions preserve their formal oxidation state Ti^{4+} . However, the adsorption of an Au adatom into a $V_{Ti_{5c}}$ vacancy site is strongly exothermic, releasing -6.38 eV (or -6.21 eV when using PBE), shown in Table IV.

This particular defective surface is found to be extremely reactive. We have computed the energy required to remove one of the oxygen atoms O_n ($n = 1, 2, 3$) in the surface layer (see Fig. 9 for site labeling). The atoms O1 and O3 are O_b atoms while the atom O2 is an in-plane oxygen. Our PBE+U values for the O1, O2, and O3 vacancy formation energies are 1.52, 2.20, and 1.36 eV respectively, which is in accord with previous PBE calculations⁷¹. For the stoichiometric, undoped $TiO_2(110)$ surface, the corresponding PBE+U value of E_V^O is 2.97 eV for an oxygen vacancy, V_O , in the bridging row, compared to O1 and O3 here. These values suggest that substituting a surface Ti_{5c} atom with an Au atom greatly weakens the binding of surface O atoms, as observed in the case of CeO_2 surfaces^{109,111}.

In Fig. 5 (E), the total DOS and PDOS of the doped $Au@V_{Ti_{5c}}$ surface is depicted in the presence of an oxygen vacancy. Here, the missing oxygen is the bridging O3 atom, O_3 atom (see Fig. 9), the vacancy formation energy of which is found to be lowest (1.36 eV) when Au substitutes a Ti atom at a Ti_{5c} site, which we call “ $Au@V_{Ti_{5c}}, V_{O3}$ ”. Concerning the electronic structure, the main difference between the two scenarios, i.e. one obtained by substituting a Ti_{5c} with an Au atom $Au@V_{Ti_{5c}}$ and the other generated by substituting a Ti_{5c} with an Au atom and by removing a surface O_b atom $Au@V_{Ti_{5c}}, V_{O3}$, is related to the reduction of the oxide substrate. As we can extract from Fig. 5 (E), in presence of a vacancy located in a neighboring bridging oxygen row, O3, the excess electron resulting from this vacancy transfers to the substrate and a filled state appears in the band gap. This gap state stems from a Ti-3d orbital, thus reducing one second-layer Ti ion to Ti^{3+} .

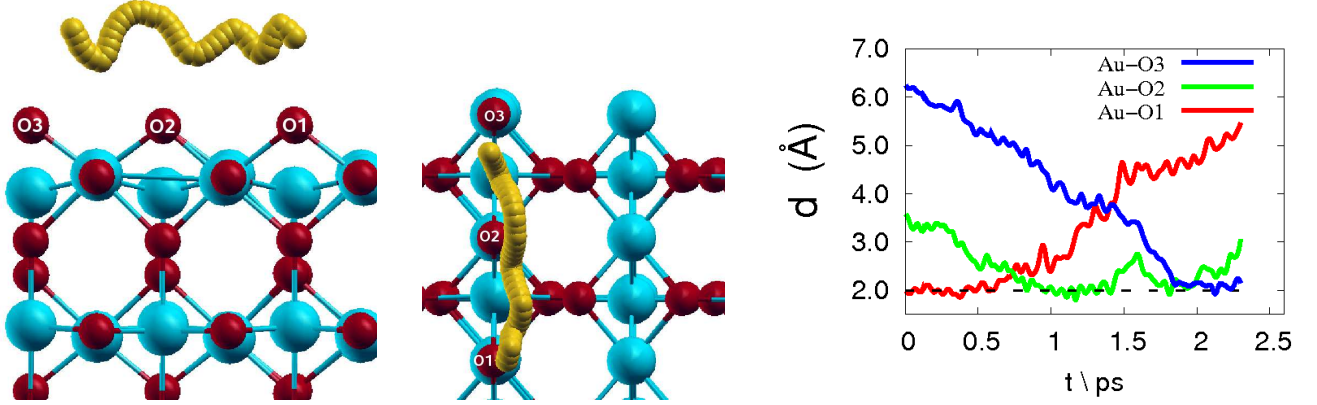


FIG. 6: Side view (left panel) and top view (central panel) of the diffusion path of the Au adatom on the stoichiometric $\text{TiO}_2(110)$ surface at 900 K. The Au atom, initially adsorbed on top of the bridging oxygen atom O1, diffuses along the O_b bridging row by hopping from one oxygen to the next, $\text{O1} \rightarrow \text{O2} \rightarrow \text{O3}$, as visualized by the worm-like trajectory. The right panel shows the time evolution of the Au- O_n ($n=1,2,3$) bond lengths; the dashed line at 2.00 Å refers to the optimized equilibrium Au-O bond length.

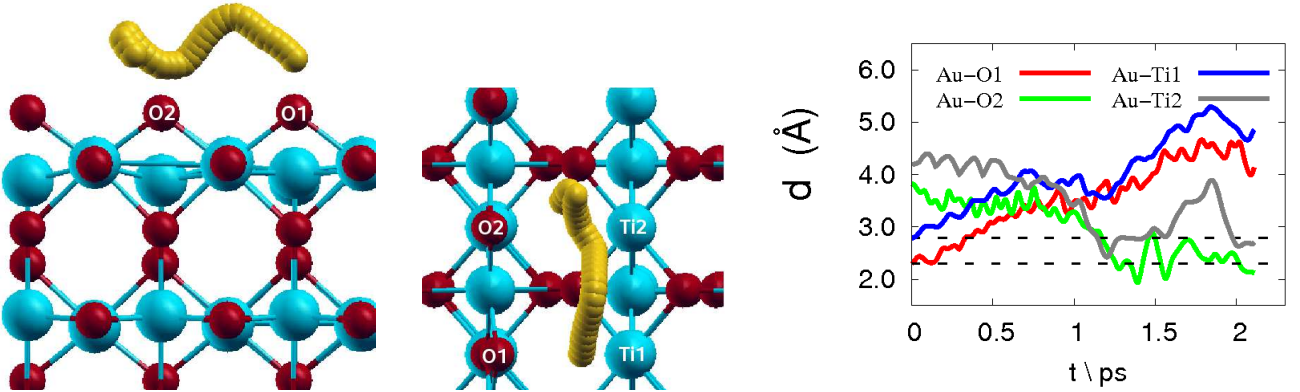


FIG. 7: Side view (left panel) and top view (central panel) of the diffusion path of the Au adatom on the stoichiometric $\text{TiO}_2(110)$ surface at 900 K. The Au atom, initially adsorbed on a bridge site between the O1 and Ti1 atoms, diffuses by hopping in between pairs of nearest-neighbor O_b bridge and Ti_{5c} atoms as visualized by the worm-like trajectory. The right panel shows the time evolution of the Au- O_n and Au- Ti_n ($n=1,2$) bond lengths; the dashed lines at 2.30 and 2.80 Å refer to the optimized equilibrium Au-O and Au-Ti bond lengths, respectively.

E. *Ab initio* thermodynamics of defective Au/ $\text{TiO}_2(110)$ surfaces

The effects of temperature and pressure on the relative stability of Au/ TiO_2 metal/oxide surfaces have been taken into account by employing the formalism of approximate *ab initio* thermodynamics, as sketched in Sec. II. To this end, we compute the free energies of Au adsorption, $\Delta G_{\text{ads}}(T, p)$ as given by Eq. (6), and report them in Fig. 10 as a function of the O chemical potential including a conversion to oxygen partial pressures at several relevant temperatures. These free energies are measured relative to the stoichiometric surface and therefore include the free energy cost of creating whatever vacancy

the gold atom may be associated with.

As highlighted by the colors in Fig. 10, it is possible to identify four thermodynamically stable phases. The first phase, which holds for values of $\mu_{\text{O}} > -1.35$ eV, corresponds to the scenario where a surface Ti_{5c} atom has been replaced by an Au adatom, denoted “Au@ $\text{V}_{\text{Ti}_{5c}}$ ”. In oxidative environments, and at the reference conditions that are traditionally used in most computational studies, this structure becomes the thermodynamically most stable one. The second most stable structure thermodynamically is the one obtained by removing a surface O atom from a bridging row based on the Au@ $\text{V}_{\text{Ti}_{5c}}$ structure described above, which is called “Au@ $\text{V}_{\text{Ti}_{5c}}, \text{V}_{\text{O}_3}$ ” since the missing O_b atom is the O3

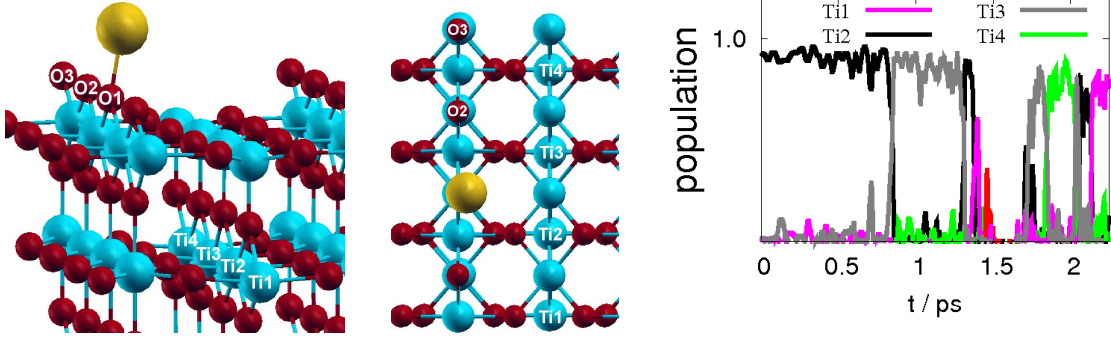


FIG. 8: Side view (left panel) and top view (central panel) of the Au adatom adsorbed on top of the surface bridging oxygen atom O1, which served as the initial configuration for the migration path depicted in Fig. 6. Right panel: Corresponding time evolution of the fractional occupation number of particular Ti-3d orbitals at specific sites, as indicated; populations of about 0 and 1 correspond to Ti^{4+} and Ti^{3+} , respectively. At $t = 0$ ps, the Au adatom is bound to O1 and the excess charge is fully localized in the second subsurface layer at the Ti2 site.

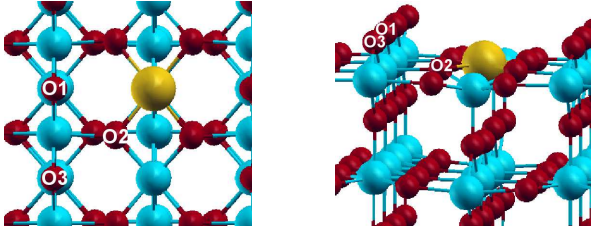


FIG. 9: Ball and stick model of an $Au_xTi_{(1-x)}O_2$ system obtained by substituting a surface Ti_{5c} atom by an Au adatom in side (left) and top (right) views.

atom (refer to Fig. 9) We have shown that the PBE+U energy required for removing the O3 oxygen atom, i.e. the vacancy formation energy E_V^{O3} , from the surface of the $Au@V_{Ti_{5c}}$ structure amounts to 1.36 eV. This is significantly lower than the required energy of 2.97 eV to remove an O_b atom from the ideal, stoichiometric TiO_2 surface. Therefore the $TiO_2(110)$ oxide surface becomes a better oxidant when doped with gold.

As demonstrated in Fig. 10, the $Au@V_{Ti_{5c}}, V_{O3}$ surface structure becomes thermodynamically stable for $-1.79 \text{ eV} < \mu_O < -1.35 \text{ eV}$. It turns out that these two defective surface structures, $Au@V_{Ti_{5c}}$ and $Au@V_{Ti_{5c}}, V_{O3}$, are thermodynamically stable in a wide range of temperatures T and pressures p that are relevant for applications in the realm of catalysis. In contrast, the adsorption of Au adatoms on the stoichiometric $TiO_2(110)$ surface is thermodynamically stable only in a quite narrow range of values of the O chemical potential of $-2.05 \text{ eV} < \mu_O < -1.79 \text{ eV}$. Finally, the adsorption of Au adatoms on O vacancies becomes thermodynamically stable for values of $\mu_O < -2.05 \text{ eV}$. We therefore conclude that under O-rich conditions, the thermodynamically most stable structure is the defective surface structure $Au@V_{Ti_{5c}}$ obtained by substituting a surface

Ti_{5c} atom with an Au adatom, while under Ti-rich conditions, the Au adatoms are preferentially adsorbed at O vacancies.

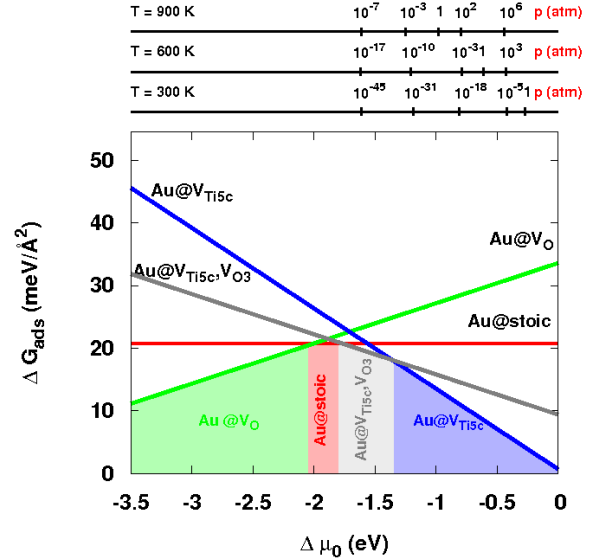


FIG. 10: Free energy $\Delta G_{\text{ads}}(T, p)$ for Au adsorption on stoichiometric and defective $TiO_2(110)$ surfaces as a function of the oxygen chemical potential $\Delta\mu_O$; see text for the four different phases. Conversion to oxygen partial pressures p (upper axes) has been carried out at constant temperatures of $T = 300, 600, \text{ and } 900 \text{ K}$ (see text).

V. GOLD-PROMOTED TITANIA: INTERACTIONS WITH CO PROBE MOLECULES

A. CO molecular adsorption on Au/TiO₂(110) surfaces

We have shown that our calculations predict the two most stable adsorption sites of an Au adatom adsorbed on the stoichiometric TiO₂(110) surface, differing energetically by only ~ 0.1 eV. The lowest energy configuration is that with the Au adatom adsorbed onto a bridge site between a surface O_b atom and a first-layer Ti_{5c} atom. A detailed analysis of the electronic structure of this configuration shows that all Ti ions belonging to the substrate preserve their formal oxidation state Ti⁴⁺. The other stable structure consists of an Au adatom sitting on top of an O_b atom of the (110) surface. The metal adsorption on an O_b top site induces a strong charge rearrangement at the metal/oxide contact and entails the reduction of a second-layer Ti ion which becomes formally Ti³⁺.

Using these preferred structures, we now study their interaction with a CO admolecule. A CO molecule is placed end-on at 2.5 Å above the Au adatoms. The adsorption of the CO molecule on an Au adatom adsorbed at an O_b site is found to be strongly exothermic, releasing -2.66 eV (-2.33 eV using PBE; see Table IV). This is in accord with earlier calculations⁶⁸. In this configuration, the CO molecule is aligned with the Au adatom and oriented normal to the surface (see Fig. 11 (F)). The computed value of the C–O bond length is 1.15 Å compared to a value of 1.14 Å of an isolated CO molecule using the same approach. The PBE+U (PBE) value of the distance between the Au atom and the substrate O_b atom to which it is bonded is 1.98 Å (1.97 Å), while the Au to C distance is 1.88 Å (1.88 Å). Analysis of the PDOS (see Fig. 11 (F)) reveals that at this Au/TiO₂ contact, only one Ti³⁺ ion is present before and after adsorption, and that the excess charge populating the substrate occupies the same second-layer Ti-3*d* orbital. Therefore, the charge redistribution due to adsorbing a CO molecule does not further reduce the oxide support. However, the bonding charge analysis (also displayed in Fig. 11 (F)) shows that the Au adatom is involved in charge depletion (blue areas), while both the C and O atoms accumulate the resulting excess charge (red areas).

We now consider the interaction between a CO molecule and the Au atom adsorbed onto the bridge site. Again, the mechanism is exothermic by -2.27 eV (or -2.17 eV when using PBE instead of PBE+U). In this configuration, the CO molecule is bonded to the Au atom and the C–O bond length is 1.15 Å as in the previous case. Here, however, the CO–Au structure is found to be tilted with respect to the surface at an angle of about 60° (see Fig. 11 (G)). The PBE+U (PBE) values of the distances between the Au adatom and the Ti_{5c} atom before and after the adsorption of molecular CO are 2.79 (2.88)

and 3.90 Å (3.88 Å), respectively, while the distances between the metal and the O bridging atom before and after CO adsorption are 2.30 (2.39) and 1.99 Å (2.01 Å), respectively. The analysis of the PDOS as depicted in Fig. 11 (G) shows, in this case, that at the Au/TiO₂ contact, the charge redistribution reduces the oxide support, contrary to the previous scenario. We recall that when Au is adsorbed onto a bridge site, all the substrate Ti ions preserve their formal Ti⁴⁺ oxidation state. Upon CO adsorption onto the Au atom occupying a bridge position, one Ti ion is reduced. The additionally reduced Ti³⁺ ion, which belongs to the first TiO₂ layer, is precisely the ion that forms a bond with the Au in the bridge configuration before CO adsorption.

The configuration in Fig. 11 (G), where the CO–Au structure is tilted by $\sim 60^\circ$ with respect to the substrate, is used as an initial condition for a short AIMD run at room temperature in order to probe dynamical instabilities. In less than 0.4 ps, the CO–Au complex bends and sits perpendicular to the surface, therefore recovering the structure obtained upon molecular CO adsorption on gold sitting on top of an O_b atom. The difference in the binding energies for CO molecule adsorption on the top and bridge configurations described above can be attributed in part to the tilting of the Au–CO complex with respect to the surface plane. More important, however, is the position of the reduced Ti³⁺ site. Previous studies^{13,79} on charge localization induced by O_b vacancies on TiO₂ surfaces have shown that excess electrons, which are trapped at specific Ti sites, migrate easily by phonon-assisted hopping to other Ti atoms, thus exploring different electronic structure topologies¹³. In particular, it was found that the most stable sites for charge localization belong to the second subsurface layer under Ti_{5c} rows. The topologies where the excess charge is shared between surface Ti_{5c} atoms and second or third subsurface layer sites below Ti_{5c} rows were found to be about 0.2–0.3 and 0.3–0.4 eV higher in energy, respectively. It is therefore conceivable that we would observe a similar dynamics for excess charge de- and re-localization.

B. CO adsorption on Au₁/TiO_(2-x)(110) and Au₂/TiO_(2-x)(110) surfaces

The interaction between a CO molecule and a single Au adatom adsorbed at a bridging site or on top of an O_b atom on the TiO₂(110) surface has been investigated above. We now concentrate on the interaction between CO molecule and Au adatom adsorbed at a bridging O vacancy. It has been shown that the metal adatom strongly interacts with this reduced oxide support. The resulting Au^{δ-} adatom is highly stable, considering its binding energy of -1.54 eV. Our calculations predict a fairly weak interaction between molecular CO and the Au^{δ-} adatom. The CO molecule initially located end-on at 2.5 Å above the Au^{δ-} species is found to bind with about -0.41 eV. This binding energy is close to an order

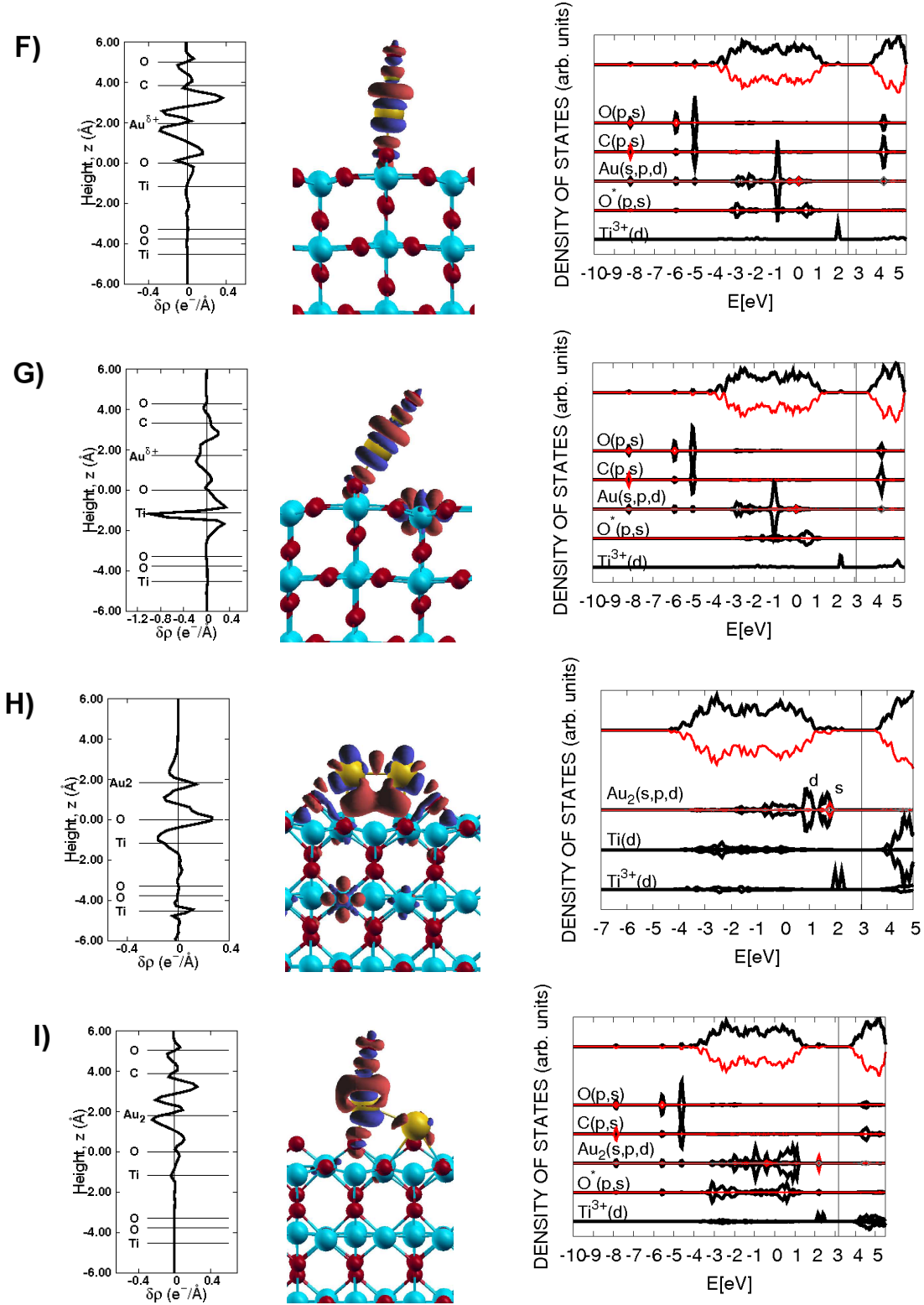


FIG. 11: Electronic structure analyses (based on the PBE+U approach) of (F) a CO molecule adsorbed on a supported Au adatom (originally the Au atom was adsorbed at a bridging O atom) on the TiO₂(110) surface, (G) a CO molecule adsorbed on a supported Au adatom (originally the Au atom was adsorbed between a bridging O atom and a Ti_{5c} atom) on the TiO₂(110) surface, (H) of the Au₂ dimer adsorbed onto surface and (I) a CO molecule bonded to an Au₂ dimer adsorbed onto a surface O vacancy on the TiO₂(110) surface. The left panel represents the bonding charge $\delta\rho(z)$ integrated over planes perpendicular to the surface and plotted as a function of the height from the surface. The central panel displays the bonding charge $\Delta\rho(\vec{r})$ at an isovalue of $\pm 0.06 |e|/\text{\AA}^3$ where electron accumulation and depletion are represented by red and blue areas, respectively. The right panel shows the total DOS and atom resolved projected DOS (PDOS), as indicated, where energies are with respect to the Fermi level, which is marked by a solid vertical line.

of magnitude lower than the binding energy of the positively charged Au adatom adsorbed on the stoichiometric $\text{TiO}_2(110)$ surface, which binds with -2.66 eV.

Our calculations show that while positively charged $\text{Au}^{\delta+}$ ions supported on the $\text{TiO}_2(110)$ surface are shown to activate molecular CO, negatively charged $\text{Au}^{\delta-}$ adspecies, which are incorporated into surface O vacancies, interact only weakly with CO adsorbates. This is in line with the scenario of Au adsorbed on the CeO_2 substrate^{109,110}, where it has been shown that the higher stability of Au adatoms adsorbed onto surface is the basis of the deactivation mechanism during CO oxidation. The oxidation mechanism proposed¹⁰⁹ involves three steps: the spillover of the CO molecule, the actual oxidation via a lattice oxygen atom leading to CO_2 desorption, and the diffusion of the Au adatom into the newly formed O vacancy, which results in negatively charged $\text{Au}^{\delta-}$ adspecies that prevents the adsorption of molecular CO. Since the present AIMD simulations have shown that Au adatoms diffuse rather easily on the stoichiometric $\text{TiO}_2(110)$ surface, we would expect a deactivation process with titania similar to what was observed on the ceria surface.

Despite the fact that CO only weakly interacts with negatively charged $\text{Au}^{\delta-}$ adspecies, several theoretical and experimental studies suggest that V_O vacancies in bridging oxygen rows, O_b , are active nucleation sites for Au_n clusters on the $\text{TiO}_2(110)$ surface^{7,113,114}. It is therefore expected that nucleation and growth of Au_n clusters on the rutile surface is intimately related to the presence of surface oxygen vacancies. To get a glimpse, we next investigated the limiting case of a gold dimer, Au_2 , adsorbed at an O_b vacancy. The optimized structure of an Au_2 dimer adsorbed onto a surface bridging O vacancy is depicted in Fig. 12 (a). The computed value of the adsorption energy of Au_2 on the reduced $\text{TiO}_2(110)$ surface, calculated with respect to the isolated Au_2 molecule, is -1.17 eV (-1.19 eV with PBE). The adsorption mechanism induces reduction of an additional Ti ion, leading to a gold dimer into an O vacancy and two second-layer Ti^{3+} ions (see Fig. 11 (H)). The two gold atoms are located 1.20 Å above the O vacancy site, whereas the distances between the Au atoms and the nearest-neighbor Ti atoms are 2.80 Å and the Au–Au distance amounts to 2.51 Å compared to 2.53 Å of the isolated gold dimer using the same method.

Next, a CO molecule is positioned above the Au_2 dimer adsorbed onto the surface O vacancy. After relaxation, the CO molecule reaches the most stable configuration of Fig. 12 (b). The computed binding energy is -1.22 eV (-1.00 eV using PBE), in good agreement with previous studies⁶⁸. This value is about half of that obtained for adsorption of CO on a single Au adatom adsorbed on the stoichiometric surface (-2.66 eV) but distinctly lower than the energy calculated on the $\text{Au}/\text{TiO}_{(2-x)}$ surface (-0.40 eV). We therefore find that a cluster as small as Au_2 nucleated at an O vacancy on the reduced $\text{TiO}_2(110)$ surface favors the formation of stable CO ad-

sorbates. Specifically, the CO molecule binds to the Au atom that is farthest from the O vacancy and the Au–Au distance elongates from 2.51 to 2.78 Å. The interaction between CO and the metal oxide does not induce further reduction of the substrate; before and after adsorption, two reduced Ti^{3+} ions are present (see Fig. 11 (I)). In Fig. 12, we plot the spin density of the Au_2 dimer adsorbed on the reduced TiO_2 surface (a) and the spin density after adsorbing a CO molecule to this $\text{Au}_2/\text{TiO}_{(2-x)}$ metal/oxide substrate (b). In each panel, we can see that both Ti^{3+} ions belong to subsurface layer sites below Ti_{5c} rows.

It is clear from these calculations that a gold “cluster” as small as the Au_2 dimer adsorbed onto a bridging O vacancy leads to a promoted support that strongly binds to molecular CO. Furthermore, the step from one to two gold atoms greatly changes the electronic properties, thus lending support to the general view that the reactivity of gold nanoparticles nucleated at O vacancies is strongly size dependent.

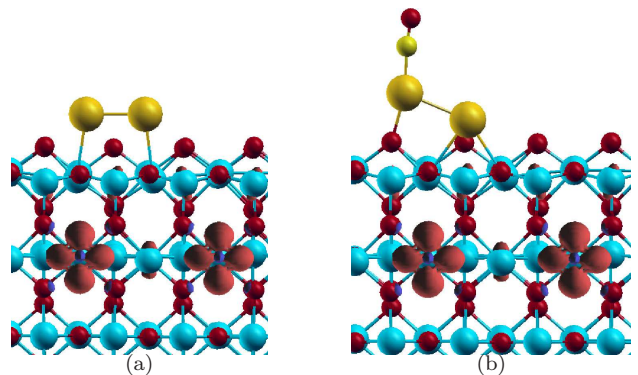


FIG. 12: Spin density at $\pm 0.005 |e|/\text{\AA}^3$ of the Au_2 dimer adsorbed onto a surface O vacancy on the $\text{TiO}_2(110)$ surface (a), and the same system after coadsorbing a CO molecule (b); see text.

VI. CONCLUSIONS AND OUTLOOK

We have performed periodic density functional based calculations that account for the on-site Coulomb interaction via a Hubbard correction (“GGA+U”) on stoichiometric, reduced, and gold-promoted rutile $\text{TiO}_2(110)$ surfaces. Structure optimizations, *ab initio* thermodynamics calculations, and *ab initio* molecular dynamics simulations have been carried out both using PBE+U and plain PBE in order to provide a broad picture on the interactions of these surfaces with several catalytically important molecules.

In agreement with plain PBE calculations and experimental results, we find that H atoms preferentially adsorb on surface O_b atoms of the stoichiometric surface. Adsorption of hydrogen results in its reduction and transfer

of close to one electron per H atom to the substrate. Using PBE+U, however, the electron transferred by a single H atom into the substrate localizes preferentially at second-layer Ti sites (whereas plain PBE yields a delocalized state). Both PBE+U and PBE calculations show a decrease in the adsorption energy as a function of coverage and a maximum coverage of about 60–70%. Oxygen vacancies are the preferred adsorption sites for H₂O dissociation and similar values for the adsorption energies of water are obtained with and without the Hubbard correction. Our PBE+U calculations predict the presence of two reduced Ti³⁺ ions before and after the adsorption of water, indicating that the adsorption of water does not further reduce the support (whereas plain PBE again yields delocalized excess electrons).

Akin to plain PBE calculations, PBE+U predicts a weak interaction between CO molecules and the reduced TiO₂ substrate. The data indicate that CO adsorbs at both oxygen vacancies in the bridging surface rows, O_b, and fivefold coordinated titania sites in the first layer, Ti_{5c}. While PBE calculations give similar energy values for CO at oxygen vacancies and at Ti_{5c}, PBE+U calculations show that the adsorption of CO at those Ti_{5c} sites which are nearest neighbors of the oxygen vacancies is energetically disfavored. Upon CO adsorption on the reduced oxide, the resulting charge redistribution does not reduce further the titania substrate.

Addressing next the interaction of titania with gold, both PBE+U and PBE calculations predict two most stable adsorption sites for Au adatom adsorption on the stoichiometric TiO₂ surface. On the one hand, once an Au adatom is adsorbed at a bridge site between a surface O_b atom and a first-layer Ti_{5c} atom, PBE+U suggests that all the Ti ions belonging to the substrate preserve their formal oxidation state Ti⁴⁺, indicating a very weak oxidation of Au. On the other hand, if the Au adatom is adsorbed on top of an O_b atom, a net charge transfer from the metal to surface, leading to a positively charged Au^{δ+}, is observed. In this case, the metal adsorption entails the reduction of a second-layer Ti ion, which formally becomes Ti³⁺. *Ab initio* molecular dynamics reveals that gold adatoms on stoichiometric TiO₂(110) are very mobile. They are found to migrate easily along the [001] direction, either along the top of bridging oxygen rows or around the area between such rows. In the former case, we observe an interesting subsurface charge delocalization and relocalization dynamics of the excess

charge.

Promotion of the (110) rutile surface via adsorption of gold atoms or substitution of Ti by Au results in a system with greatly changed electronic properties and thus modified reactivities in the realm of heterogeneous catalysis. This is traced back to the oxidation state of the gold adatoms, which is determined by the site at which the Au atom is adsorbed as well as by the stoichiometry of the substrate. Isolated Au atoms supported by the stoichiometric TiO₂ surfaces are shown to induce a significant charge redistribution at the metal/oxide contact. The calculations, both PBE+U and PBE, show positively charged Au^{δ+} adspecies supported on the stoichiometric surface which activate CO admolecules. In stark contrast, the negatively charged Au^{δ-} adspecies, which are incorporated into surface O_b vacancies, interact only weakly with the same CO molecules. We have shown that structures obtained by substituting a first-layer Ti_{5c} ion with an Au atom weakens the bond of surface O atoms, akin to recent observations with ceria. *Ab initio* thermodynamics mappings of the surface phase diagram predict that the “Au@V_{Ti5c}” and “Au@V_{Ti5c}, V_{O3}” of temperatures and pressures relevant for catalytic applications. Finally, we have shown that although a single Au adatom bound to a surface O vacancy weakly binds CO, a second gold atom adsorbed simultaneously into the O vacancy leads to the formation of a gold dimer, Au₂, featuring distinctly different electronic and binding properties.

We expect that these insights will be of great help in understanding the catalytic activity of gold-promoted titania interfaces with liquid water as used in selective oxidation reactions of more complex molecules.

Acknowledgments

We are grateful to Bernd Meyer and Martin Muhler for fruitful discussions. This work has been supported by the German Research Foundation (DFG) via the Collaborative Research Center SFB 558 “Metal–Substrate Interactions in Heterogeneous Catalysis,” by Research Department “Interfacial Systems Chemistry” (RD IFSC), and by Fonds der Chemischen Industrie (FCI). Computational resources were provided by NIC (Jülich), BOVI-LAB@RUB (Bochum), and by RV–NRW.

* Electronic address: matteo.farnesi@theochem.rub.de

† Present address: Helmholtz Centre Potsdam, Telegrafenberg, 14473 Potsdam, Germany

¹ C. T. Campbell, A. W. Grant, D. E. Starr, S. C. Parker, and V. A. Bondzie, *Top. Catal.* **14**, 43 (2001).

² U. Diebold, *Surf. Sci. Rep.* **48**, 53 (2003).

³ M. V. Ganduglia-Pirovano, A. Hofmann, and J. Sauer, *Surf. Sci. Rep.* **62**, 219 (2007).

⁴ G. Pacchioni, *J. Chem. Phys.* **128**, 182505 (2008).

⁵ F. Besenbacher, J. V. Lauritsen, T. R. Linderoth, E. Lægsgaard, R. T. Vang, and S. Wendt, *Surf. Sci.* **603**, 1315 (2009).

⁶ B. O’Regan and M. Grätzel, *Nature* **353**, 737 (1991).

⁷ D. Matthey, J. G. Wang, S. Wendt, J. Matthiesen, R. Schaub, E. Laegsgaard, B. Hammer, and F. Besenbacher, *Science* **315**, 1692 (2007).

- ⁸ H. Imagawa, T. Tanaka, N. Takahashi, S. Matsunaga, A. Suda, H. Shinjoh *et al.*, *J. Catal.* **251**, 315 (2007).
- ⁹ P. M. Kowalski, B. Meyer, and D. Marx, *Phys. Rev. B* **79**, 115410 (2009).
- ¹⁰ Z. Dohnalek, I. Lyubinetsky, and R. Rousseau, *Prog. Surf. Sci.* **85**, 161 (2010).
- ¹¹ V. E. Henrich, G. Dresselhaus, and H. J. Zeiger, *Phys. Rev. Lett.* **36**, 1335 (1976).
- ¹² C. T. Campbell, S. C. Parker, and D. E. Starr, *Science* **298**, 811 (2002).
- ¹³ P. M. Kowalski, M. Farnesi Camellone, N. N. Nair, B. Meyer, and D. Marx, *Phys. Rev. Lett.* **105**, 146405 (2010).
- ¹⁴ V. E. Henrich and R. L. Kurtz, *Phys. Rev. B* **23** 6280 (1981).
- ¹⁵ M. Kunat, U. Burghaus, and Ch. Wöll, *Phys. Chem. Chem. Phys.* **6**, 4203 (2004).
- ¹⁶ S. Suzuki, K. I. Fukui, H. Onishi, and Y. Iwasawa, *Phys. Rev. Lett.* **84**, 2156 (2000).
- ¹⁷ T. Fujino, M. Katayama, K. Inudzuka, T. Okuno, and K. Oura, *Appl. Phys. Lett.* **79**, 2716 (2001).
- ¹⁸ X.-L. Yin, M. Calatayud, H. Qiu, Y. Wang, A. Birkner, C. Minot, and Ch. Wöll, *ChemPhysChem* **9**, 253 (2008).
- ¹⁹ C. Sun, L.-M. Liu, A. Selloni, G. Q. Lu, and S. C. Smith, *J. Mat. Chem.* **20**, 10319 (2010).
- ²⁰ M. B. Hugenschmidt, L. Gamble, and C. T. Campbell, *Surf. Sci.* **302**, 329 (1994).
- ²¹ D. Brinkley, M. Dietrich, T. Engel, P. Farral, G. Gantner, A. Schafer, and A. Szuchmaher, *Surf. Sci.* **395**, 292 (1998).
- ²² R. L. Kurtz, R. Sockbauer, T. E. Madey, E. Roman, and J. L. De Segovia, *Surf. Sci.* **218**, 178 (1989).
- ²³ J. Goniakowski and M. J. Gillan, *Surf. Sci.* **350**, 145 (1996).
- ²⁴ P. J. D. Lindan, N. M. Harrison, J. M. Holender, and M. J. Gillan, *Chem. Phys. Lett.* **261**, 246 (1996).
- ²⁵ S. P. Bates, G. Kresse, and M. J. Gillan, *Surf. Sci.* **409**, 336 (1998).
- ²⁶ P. J. Lindan, N. M. Harrison, and M. J. Gillan, *Phys. Rev. Lett.* **80**, 762 (1998).
- ²⁷ E. V. Stefanovich and T. N. Truong, *Chem. Phys. Lett.* **299**, 623 (1999).
- ²⁸ W. Langel, *Surf. Sci.* **496**, 141 (2002).
- ²⁹ C. Zhang and P. J. D. Lindan, *J. Chem. Phys.* **118**, 4620, (2003).
- ³⁰ P. J. D. Lindan and C. Zhang, *Phys. Rev. B* **72**, 075439 (2005).
- ³¹ L. A. Harris and A. A. Quong, *Phys. Rev. Lett.* **93**, 086105 (2004); P. J. D. Lindan and C. Zhang, *ibid.* **95**, 029601, (2005); L. A. Harris and A. A. Quong, *ibid.* **95**, 029602 (2005).
- ³² H. Perron, J. Vandenborre, C. Domain, R. Drot, J. Roques, E. Simoni, J.-J. Ehrhardt, and H. Catalette, *Surf. Sci.* **601**, 518 (2007).
- ³³ L.-M. Liu, C. Zhang, G. Thornton, and A. Michaelides, *Phys. Rev. B* **82**, 161415(R) (2010).
- ³⁴ M. A. Henderson, *Surf. Sci.* **355**, 151 (1996).
- ³⁵ R. Schaub, P. Thosttrup, N. Lopez, E. Lægsgaard, I. Stensgaard, J. K. Nørskov, and F. Besenbacher, *Phys. Rev. Lett.* **87**, 266104 (2001).
- ³⁶ S. Wendt, R. Schaub, J. Matthiesen, E. K. Vestergaard, E. Wahlström, M. D. Rasmussen, P. Thorstrup, L. M. Molina, E. Lægsgaard, I. Stensgaard, B. Hammer, and F. Besenbacher, *Surf. Sci.* **598**, 226 (2005).
- ³⁷ Q. Fu, H. Saltsburg, and M. Flytzani-Stephanopoulos, *Science* **301**, 935 (2003).
- ³⁸ Y. Sato, M. Koizumi, T. Miyao, and S. Naito, *Catal. Today* **111**, 164 (2006).
- ³⁹ M. Kunat, F. Traeger, D. Silber, H. Qiu, Y. Wang, A. C. van Veen, Ch. Wöll, P. M. Kowalski, B. Meyer, C. Hättig, and D. Marx, *J. Chem. Phys.* **130**, 144703 (2009).
- ⁴⁰ A. Linsebliger, G. Lu, and J. T. Yates, *J. Chem. Phys.* **103**, 9438 (1995).
- ⁴¹ Z. Dohnálek, J. Kim, O. Bondarchuck, J. M. White, and B. D. J. Kay, *Phys. Chem. B* **110**, 6229 (2006).
- ⁴² G. Pacchioni, A. M. Ferrari, and P. S. Bagus, *Surf. Sci.* **350**, 159 (1996).
- ⁴³ M. Casarin, C. Maccato, and A. Vittadini, *J. Phys. Chem. B* **102**, 10745 (1998).
- ⁴⁴ D. Pillay and G. S. Hwang, *J. Chem. Phys.* **125**, 144706 (2006).
- ⁴⁵ W. Göpel, G. Rocker, and R. Feierabend, *Phys. Rev. B* **28**, 3427 (1983).
- ⁴⁶ G. Rocker and W. Göpel, *Surf. Sci.* **175**, L675 (1986).
- ⁴⁷ M. Menetrey, A. Markovits, and C. Minot, *Surf. Sci.* **524**, 49 (2003).
- ⁴⁸ H. Kobayashi and M. Yamaguchi, *Surf. Sci.* **214**, 466 (1989).
- ⁴⁹ M. Haruta, N. Yamada, T. Kobayashi, and S. Iijima, *J. Catal.* **115**, 301 (1989).
- ⁵⁰ S. C. Parker, A. W. Grant, A. Bondzie, and C. T. Campbell, *Surf. Sci.*, **441**, 10 (1999).
- ⁵¹ J. D. Grunwaldt, C. Kiener, C. Wogerbauer, and A. Baiker, *J. Catal.* **181**, 223 (1999).
- ⁵² Z.-P. Liu, X.-P. Gong, J. Kohanoff, C. Sanchez, and P. Hu, *Phys. Rev. Lett.* **91**, 266102 (2003)
- ⁵³ G. Mills, M. S. Gordon, and H. Metiu, *J. Chem. Phys.* **118**, 4198 (2003).
- ⁵⁴ M. Haruta, *Catal. Today* **36**, 153 (1997).
- ⁵⁵ G. C. Bond and D. T. Thompson, *Cat. Rev. Sci. Eng.* **41**, 319 (1999).
- ⁵⁶ N. Lopez and J. Nørskov, *J. Am. Chem. Soc.* **124**, 11262 (2002).
- ⁵⁷ N. Lopez, T. V. W. Janssens, B. S. Clausen, Y. Xu, M. Mavrikakis, T. Bligaard, and J. Nørskov, *J. Catal.* **223**, 232 (2004).
- ⁵⁸ M. Valden, X. Lai, and D. W. Goodman, *Science* **281**, 1647 (1998).
- ⁵⁹ M. Haruta, *Chem. Rec.* **3**, 75 (2003).
- ⁶⁰ L. M. Molina, M. D. Rasmussen, and B. Hammer, *J. Chem. Phys.* **120**, 7673 (2004).
- ⁶¹ Z. Yang, R. Wu, and D. W. Goodman, *Phys. Rev. B* **61**, 14066 (2000).
- ⁶² L. Giordano, G. Pacchioni, T. Bredow, and J. F. Sanz, *Surf. Sci.* **471**, 21 (2001).
- ⁶³ N. Lopez and J. K. Nørskov, *Surf. Sci.* **515**, 175 (2002).
- ⁶⁴ A. Vijay, G. Mills, and H. Metiu, *J. Chem. Phys.* **118**, 6536 (2003).
- ⁶⁵ K. Okazaki, Y. Morikawa, S. Tanaka, K. Tanaka, and M. Kohyama, *Phys. Rev. B* **69**, 235404 (2004).
- ⁶⁶ D. Pillay and G. S. Wang, *Phys. Rev. B* **72**, 205422 (2005).
- ⁶⁷ H. Iddir, S. Ögöt, N. D. Browning, and M. M. Disko, *Phys. Rev. B* **72**, 081407(R) (2005).
- ⁶⁸ A. S. Wörz, U. Heiz, F. Cinquini, and G. Pacchioni, *J. Phys. Chem. B* **109**, 18418 (2005).
- ⁶⁹ J. Graciani, A. Nambu, J. Evans, J. A. Rodriguez, and J. Fdez. Sanz, *J. Am. Chem. Soc.* **130**, 12056 (2008).
- ⁷⁰ H. Shi, M. Kohyama, S. Tanaka, and S. Takeda, *Phys.*

- Rev. B **80**, 155413 (2009).
- ⁷¹ S. Chrézien and H. Metiu, Catal. Lett. **107**, 143 (2006).
- ⁷² L. Hedin, Phys. Rev. **139**, A796 (1967).
- ⁷³ R. Resta, Phys. Rev. Lett. **80**, 1800 (1998); C. Sgiarovello, M. Peressi, and R. Resta, Phys. Rev. B **64**, 115202 (2001).
- ⁷⁴ M. S. Hybertsen and S. G. Louie, Phys. Rev. Lett. **55**, 1418 (1985).
- ⁷⁵ W. Metzner and D. Vollhardt, Phys. Rev. Lett. **62**, 324 (1989); A. Georges, G. Kotliar, W. Krauth, and M. J. Rozenberg, Rev. Mod. Phys. **68**, 13 (1996).
- ⁷⁶ A. Filippetti and N. A. Spaldin, Phys. Rev. B **67**, 125109 (2003).
- ⁷⁷ V. I. Anisimov, J. Zaanen, and O. K. Andersen, Phys. Rev. B **44**, 943 (1991); V. I. Anisimov, M. A. Korotin, J. Zaanen, and O. K. Andersen, Phys. Rev. Lett. **68**, 343 (1992); V. I. Anisimov, I. V. Solovyev, M. A. Korotin, M. T. Czyzyk, and G. A. Sawatzky, Phys. Rev. B **48**, 16 929 (1993).
- ⁷⁸ A. D. Becke, J. Chem. Phys. **98**, 1372 (1993).
- ⁷⁹ N. A. Deskins and M. Dupuis, Phys. Rev. B **75**, 195212 (2007).
- ⁸⁰ N. A. Deskins, R. Rousseau, and M. Dupuis, J. Phys. Chem. C **113**, 14583 (2009).
- ⁸¹ J. P. Perdew, K. Burke, and M. Ernzerhof, Phys. Rev. Lett. **77**, 3865 (1996); Phys. Rev. Lett. **78**, 1396(E) (1997).
- ⁸² D. Vanderbilt, Phys. Rev. B **41**, 7892 (1990).
- ⁸³ A. C. Papageorgious *et al.*, PNAS **107**, 2391 (2010).
- ⁸⁴ E. Finazzi, C. Di Valentin, G. Pacchioni and A. Selloni, J. Chem. Phys. **129**, 154113 (2008).
- ⁸⁵ B. J. Morgan and G. W. Watson, J. Phys. Chem. C **113**, 7322 (2009).
- ⁸⁶ B. J. Morgan and G. W. Watson, Surf. Sci. **601**, 5034 (2007).
- ⁸⁷ F. Filipone, G. Mattioli, P. Alippi, and A. Amore Bonapasta, Phys. Rev. B **80**, 245203 (2009).
- ⁸⁸ C. J. Calzado, N. C. Hernández, and J. F. Sanz, Phys. Rev. B **77**, 045118 (2008).
- ⁸⁹ M. Cococcioni and S. de Gironcoli, Phys. Rev. B **71**, 035105 (2005).
- ⁹⁰ H. J. Kulik, M. Cococcioni, D. A. Scherlis, and N. Marzari, Phys. Rev. Lett. **97**, 103001 (2006).
- ⁹¹ G. Mattoili, P. Alippi, F. Filippone, R. Caminiti, and A. A. Bonapasta, J. Chem. Phys. C **114**, 21694 (2010).
- ⁹² W. E. Pickett, S. C. Erwin, and E. C. Ethridge, Phys. Rev. B **58**, 1201 (1998).
- ⁹³ P. Giannozzi *et al.*, J. Phys.: Condens. Matter **21**, 395502 (2009); *Quantum Espresso*, www.pwscf.org.
- ⁹⁴ D. Marx and J. Hutter, *Ab Initio Molecular Dynamics: Basic Theory and Advanced Methods* (Cambridge University Press, Cambridge 2009).
- ⁹⁵ R. Car and M. Parrinello, Phys. Rev. Lett. **55**, 2471 (1985).
- ⁹⁶ J. Hutter *et al.*, CPMD, www.cpmd.org.
- ⁹⁷ E. Kaxiras, Y. Bar-Yam, J. D. Joannopoulos, and K. C. Pandey, Phys. Rev. B **35**, 9624 (1987).
- ⁹⁸ G.-X. Qian, R. M. Martin, and D. J. Chadi, Phys. Rev. B **38**, 7649 (1988).
- ⁹⁹ K. Reuter and M. Scheffler, Phys. Rev. B **65**, 035406 (2001).
- ¹⁰⁰ B. Meyer, Phys. Rev. B **69**, 045416 (2004).
- ¹⁰¹ B. Meyer, in *Computational Nanoscience: Do It Yourself!*, edited by J. Grotendorst, S. Blügel, and D. Marx (NIC, FZ Jülich 2006), pp. 411-418.
- ¹⁰² C. Di Valentin, G. Pacchioni, and A. Selloni, Phys. Rev. Lett. **97**, 166803 (2006).
- ¹⁰³ A. Tilocca, C. Di Valentin, and A. Selloni, J. Phys. Chem. B **109**, 20963 (2005).
- ¹⁰⁴ M. A. Henderson, W. S. Epling, C. H. F. Peden, and C. L. Perkins, J. Phys. Chem. B **107**, 534 (2003).
- ¹⁰⁵ P. A. Redhead, Vacuum **12**, 203 (1962).
- ¹⁰⁶ L. E. Walle, A. Borg, P. Uvdal, and A. Sandell, Phys. Rev. B **80**, 235436 (2009).
- ¹⁰⁷ X. Wu, A. Selloni, and S. K. Nayak, J. Chem. Phys. **9**, 4512 (2003).
- ¹⁰⁸ Y. Zhao, Z. Wang, X. Cui, T. Huang, B. Wang, Y. Luo, J. Yang, and J. Hou, J. Am. Chem. Soc. **131**, 7958 (2009).
- ¹⁰⁹ M. Farnesi Camellone and S. Fabris, J. Am. Chem. Soc. **131**, 10473 (2009).
- ¹¹⁰ C. Zhang, A. Michaelides, D. A. King, and S. J. Jenkis, J. Phys. Chem. **129**, 194708 (2008).
- ¹¹¹ Y. Chen, M.-H. Lee, and H. Wang, Surf. Sci. **602**, 1736 (2008).
- ¹¹² H. Jónsson, G. Mills, and K. W. Jacobsen, *Classical and Quantum Dynamics in Condensed Phase Simulations*; World Scientific: Singapore, 1998; Chapter 16, p. 385
- ¹¹³ J. G. Wang and B. Hammer, Phys. Rev. Lett. **97**, 136207 (2006).
- ¹¹⁴ E. Wahlstrom, N. Lopez, R. Schaub, P. Thostrup, A. Rønnau, A. Africh, E. Laegsgaard, J. K. Nørskov, and F. Besenbacher, Phys. Rev. Lett. **90**, 026101 (2003).